Journal of Hazardous Materials 173 (2010) 2–18

Contents lists available at ScienceDirect

Journal of Hazardous Materials

journal homepage: www.elsevier.com/locate/jhazmat

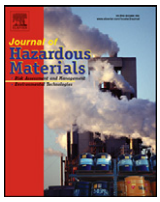

Review

General review of flashing jet studies

Geanette Polanco[a,*], Arne Erik Holdø[b,*], George Munday[c]

[a] Simón Bolívar University, Caracas, Venezuela
[b] Narvik University College, Narvik, Norway
[c] Coventry University, Coventry, UK

ARTICLE INFO

Article history:
Received 30 October 2008
Received in revised form 4 August 2009
Accepted 7 August 2009
Available online 4 September 2009

Keywords:
Flashing jet
Violent phase change
Droplets transport

ABSTRACT

The major concern on the management of superheated liquids, in industrial environments, is the large potential hazards involved in cases of any accidental release. There is a possibility that a violent phase change could take place inside the fluid released generating a flashing jet. This violent phase change might produce catastrophic consequences, such as explosions, fires or toxic exposure, in the installations and in the surroundings. The knowledge and understanding of the mechanisms involved in those releases become an important issue in the prevention of these consequences and the minimization of their impact. This work presents a comprehensive review of information about flashing processes. The review begins with a description of the single phase jet followed by a description of the two-phase flashing jet. The concepts and implications of the thermodynamic and mechanical effects on the behaviour of the jets are considered at the beginning of the review. Following the review is devoted to the classification of the different study approaches used to understand flashing processes in the past, highlighting various critical parameters on the behaviour and the hazard consequences of flashing jets. The review also contains an extensive compilation of experimental, theoretical and numerical data relating to these phenomena, which includes information on the distinct characteristics of the jet, since type of jet, velocity distribution, expansion angle and mass phase change all require individual estimation.

© 2009 Elsevier B.V. All rights reserved.

Contents

* Corresponding author.
E-mail addresses: gpolanco@usb.ve (G. Polanco), Erik.Holdo@coventry.ac.uk (A.E. Holdø), G.Munday@isaaconsult.co.uk (G. Munday).

0304-3894/$ – see front matter © 2009 Elsevier B.V. All rights reserved.
doi:10.1016/j.jhazmat.2009.08.138

1. Introduction

Superheated liquids can form two-phase mixtures upon their accidental release to the environment under ambient conditions. The potential consequences of accidental release include injuries, fatalities, serious local pollution, destruction of installations and possible evacuation from the surrounding area of the accident. The order of magnitude of the possible damages could reach millions of pounds. Some examples of fatal accidents involving superheated liquids are: the failure of a tank car of 31,409 gallons of liquefied propane in New York, 1996 [1]; the failure of a tank car contained 29,054 gallons of a propylene/propane mixture in a chemical plant located in Pasadena, Texas, 1997 [2]; and a particularly severe incident involving the derailment of 15 containers of hazardous materials along with 2 containers of hazardous residue near Eunice, Louisiana, 2000. In this last incident the derailment resulted in a release of hazardous materials resulting in explosions and fires and about 3500 people were evacuated from the surrounding area which included both domestic housing and business premises [3].

The behaviour and the characteristics of these liquid–gas mixtures and the potential for the formation of vapour–liquid aerosols during a superheated liquid release can significantly affect the hazard zone and mitigation steps that can be taken to minimize the release impact [4,5]. Calculation procedures need to be made available on which to base risk assessments for the management of hazards. However, it turns out that due to the complexity of the interaction of mechanical and thermodynamic based processes on the behaviour of the released fluid, the methodology required for realistic calculations of this problem may include a combination of an analytical approach, an empirical approach, as well as, a numerical approach. This review of our present knowledge of the behaviour of flashing jets therefore starts with a description of these jets in Section 2 and then briefly examines the thermodynamic and mechanical processes in Sections 3 and 4.

A review dwelling only on the thermodynamics and mechanics of flashing jet behaviour would not do justice to this subject. It is necessary to examine the vast data base of our current knowledge in a logical but all embracing way. To this end we have set out the remainder of the review in three sections. Section 5 reviews our knowledge on the basis of the way in which the differing phenomena in the flashing process can be characterized. Then in Sections 6 and 7 we look at the models which have been developed to simulate these processes and the experimental work which has been done to back up the theoretical predictions.

In the information compiled in this work we employ the following convention for disperse phase elements of different materials: particles and droplets refer in turn to solid and liquid elements in gas or vapour continuous phases and bubbles refer to bubbles of vapour in a liquid continuous phase.

2. Flashing jets

Most leakage problems from breaches of containment result in the formation of jets. The jets are as a result of the difference between the internal and external pressures. In order to assess jet behaviour it is useful to first consider the behaviour of an isothermal single phase jet. A number of experimental [4], theoretical [5] and numerical [6,7] studies on the behaviour of the single phase isothermal jet have been carried out. The fundamental characterization of such jets is to be found in the study of the centreline velocity profile. This consists of a core region followed by a decay region, in which the velocity decreases proportionally to the square root of the downstream distance from the nozzle. 3D numerical simulation of jets of a circular cross-section reproduced the behaviour described, while the axisymmetric numerical approach of those jets presents a decay proportional to the reciprocal distance from the origin, as shown in Fig. 1. The angle of divergence for a round jet is between 20° and 25° and about 5° larger of a jet coming from a rectangular slit [8]. The potential core length is estimated as typically seven times the nozzle diameter from the jet exit [7]. A conical velocity distribution identifies the core region, which is related to the vena contracta effect. The velocity profile in the radial direction tends to symmetry of Gaussian shape [5].

The interaction between the jet and its surroundings involves mass, momentum and energy exchange between the jet and its surroundings. The source mass flow from the reservoir into the jet affects the internal flow patterns and the general behaviour of the jet. The entrained mass flow is proportional to the distance from the nozzle and it increases with the inflow area around the shear layer of the jet [9]. The momentum of the entrained mass compensates for the losses generated by jet propagation, thus, the momentum stays constant at any cross-section along the flow field [10].

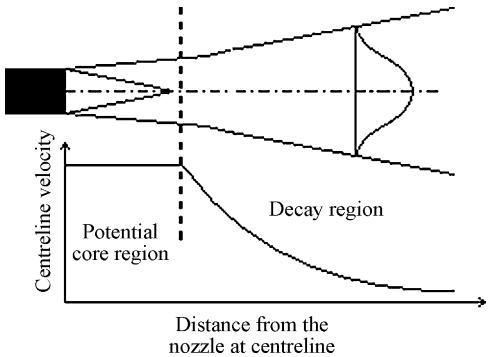

Fig. 1. Spreading of an axisymmetric jet and its velocity profile along the centreline for a isothermal single-phase jet.

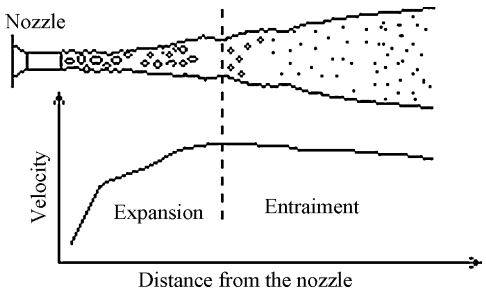

Fig. 2. Expansion–entrainment region into the jet. This figure shows the schematic velocity profile for the centreline of a flashing jet.

Moving on to the subject of this review, flashing within the jet formed at a leak of superheated liquid can occur before the fluid emerges as a jet or can occur inside the jet during the brief depressurization of the liquid. This breaks the liquid core into droplets at the same time that it emerges as an unstable jet. The flashing jet is far more complex than the single phase jet. Nevertheless, the velocity profiles at the centreline and at radial locations are used as references for experimental or empirical development work in this area.

If the liquid flashes before its exit, the section known as expansion region is characterized by the continuous breaking-up or evaporation of comparatively large droplets and large liquid ligaments. After this section, the droplet velocity decreases due to the effects of the entrainment of air. This new region is known as the entrainment region [11]. The expansion and the entrainment regions are shown in Fig. 2.

3. Thermodynamic process

The superheated condition implies that the liquid temperature is higher than its corresponding boiling temperature at its actual pressure. This condition is a metastable state. Consequently, irreversible changes in the fluid condition will occur as a fluid reaction against any significant perturbation, such as, a large pressure change.

Fig. 3 shows a typical pressure–molar volume diagram (p–v_m diagram) for a hydrocarbons fluid. Two van der Waals equation of state isothermals (filled lines) have been drawn on the diagram for temperatures $T1$ and $T2$. Each isothermal may have any of three values of molar volume for a given value of pressure. The largest value corresponds to the molar volume of saturated vapour, the smallest represents the molar volume of saturated liquid and the middle value does not have any physical meaning. Additionally, each isotherm exhibits a minimum and a maximum point ($\partial p/\partial v_m = 0$). The union of all these points is known as a spinodal line (dashed line). The superposition, on the same diagram, of the saturation line (dot dashed line), which defines the equilibrium states for the hydrocarbon under consideration, intersects with the spinodal line to create three regions inside the saturation dome. These regions are superheated liquid, unstable fluid and sub cooled vapour. The location of such regions within a flashing jet is very important for its subsequent behaviour.

The bold filled line representing isothermal changes within the saturation dome is probably more familiar to most readers; it corresponds to a true fluid in saturation conditions. A true fluid would have constant pressure for values of molar volume between the molar volume of saturated vapour and the molar volume of saturated liquid indicated by the horizontal line in Fig. 3. The value of that constant pressure for each isothermal corresponds to the geometric equal area construction.

A detailed view of the superheated liquid region is shown at the right side of Fig. 3. The coordinates (p, v_{m1}) represent saturated liquid condition and the coordinates (p, v_{m2}) represent a superheated liquid state. The temperature difference between that of the liquid, $T2$, and its saturation value, $T1$, at pressure $p1$, is defined as the degree of superheat, ΔT_{sh}, as shown by Eq. (1). T_{sat} is the saturation temperature at the actual pressure of the fluid.

$$\Delta T_{sh} = T - T_{sat} \tag{1}$$

When a system evolves from a well defined initial state to a final state by an isothermal and reversible pathway, the change in Gibbs free energy, dG, can be used to evaluate the energy content in the system. The Gibbs free energy change indicates the level of energy the fluid must overcome before experiencing a reaction, resulting from both the enthalpy and entropy contributions. The Gibbs free energy change is equal to the work exchanged by the system with its surroundings, less the work of the pressure forces, during a reversible transformation of the system from the same initial and final states as expressed in Eq. (2) [12]:

$$\mathrm{d}G = v\,\mathrm{d}p \tag{2}$$

Classical nucleation theory relies on knowledge of three fundamental processes; the thermodynamics of the phase change; the

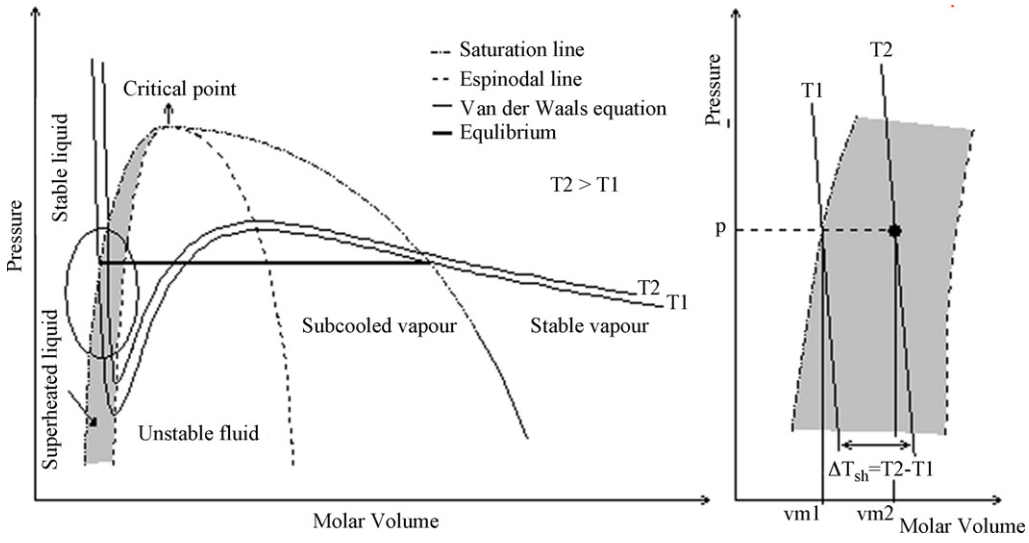

Fig. 3. Typical P–v diagram for a hydrocarbon including an inset showing details of the region associated with jet flashing.

dynamics of bubbles growth and the probability theory for the existence of molecular clusters within a liquid. There are two types of nucleation processes. These two processes have been identified as homogeneous and heterogeneous nucleation, both between the binodal points. The homogeneous nucleation process is considered as a fundamental mechanism of first-order phase transitions that will be presented in the absence of pre-existing interfaces, such as impurities inside the flow and the heterogeneous nucleation is a second-order phase transitions that takes place at preferential sites as phase boundaries or impurities like dust and requires less energy to than homogeneous nucleation. At such preferential sites, the effective surface energy is lower, thus diminished the free energy barrier and facilitating nucleation [13,14]. For a region of metastability phase separation will only proceed if a nucleus exists meanwhile homogeneous nucleation will occur between the spinodals. For flashing the transformation of the fluid can start with heterogeneous nucleation, however the rate of nucleation of the new equilibrium phase changes discontinuously as the metastable transitions are crossed. These discontinuities can be large enough that on crossing a phase transition, the rate of nucleation can jump from a negligible value to an easily observable value; that is, the transformation from one metastable phase to another can trigger nucleation of the equilibrium phase.

3.1. Homogeneous nucleation

The homogeneous nucleation process is considered as a fundamental mechanism of first-order phase transitions that occurs in the absence of pre-existing interfaces, such as impurities inside the flow. For this type of nucleation, the rate at which critical nuclei are formed is expressed by:

$$J = A \exp\left(-\frac{\Lambda G}{k_B T}\right) \tag{3}$$

where J is the number of critical nuclei formed per unit time per unit volume; A is the pre-exponential factor, ΛG is the free energy barrier to nucleation, i.e., the reversible work of formation of a critical nucleus; k_B is the Boltzmann's constant; and T is the temperature [15]. The calculation of J, therefore, entails the kinetic problem of determining A and the thermodynamic problem of determining ΛG. In this ideal case for an isothermal and reversible process, the free energy barrier to nucleation is equal to the Gibbs free energy. The pre-exponential factor and the energy barrier are given by Eqs. (4) and (5), respectively:

$$A = N\left(-\frac{3\sigma}{\pi m}\right) \tag{4}$$

$$\Lambda G = \frac{16\pi\sigma^3}{3\,\Delta\mu^2} \tag{5}$$

where N is the number density of molecules in the superheated liquid (which is a measure of the volatility of the fluid in terms related to van der Walls attractive interactions, see reference [16] for details), σ is the interfacial free energy (surface tension), $\Delta\mu$ is the liquid–vapour difference in chemical potential at the given temperature and bulk pressure.

3.2. Heterogeneous nucleation

For first-order phase transition, the molar Gibbs free energies or molar Helmholtz free energies of the two phases are equal at the transition temperature, but their first derivatives with respect to temperature and pressure (for example, specific enthalpy of transition and specific volume) are discontinuous at the transition point. The second-order transitions present continuous first derivatives of the molar Gibbs free energies or molar Helmholtz free energies, while discontinuities may exist in the second or higher derivates.

For the case of nucleation in superheated liquids within a flashing jet, the formation of cavities by density fluctuations and its relation to critically sized bubbles, formed by a sequential single-molecule process, is not obvious. The notion of a spherical macroscopic critical bubble, formed by a succession of single-molecule events, seems difficult to reconcile with actual processes occurring on a molecular scale. The heat involved in the process must be, at least, the heat necessary to induce the phase change from liquid to gas in the fluid. The nucleation process in a superheated liquid is driven by the magnitude of the statistical fluctuations compared to the critical free energy difference between two phases as stated by Frederic et al. [17]. The nucleation rate, J, is characterized by a very strong dependence on the parameters of the metastable state. For example, with the temperature rising by 1 K, the nucleation rate increases by two to five orders of magnitude [18]. Considerable research effort has been concentrated on this aspect of flashing jet behaviour. It has been established that the value of the frequency of spontaneous nucleation of a particular process will indicate if it is possible to achieve a degree of superheating before a significant quantity of bubble formation takes place. The dramatic increases in nucleation frequency portray the catastrophic change of the metastable liquid to liquid–vapour mixture [19].

3.3. Identification of nucleation mechanisms

When a liquid is undergoing a transient depressurization, by a controlled expansion of the liquid volume or by the acceleration of the flow, it is found that for an adiabatic pulse expansion a liquid may reach the homogenous nucleation limit of superheat before appreciable phase transition occurs. During the decompression the fluctuations in thermal motion can produce some vapour bubbles. The process of bubble formation and growth continuously increases the vapour content in the system until a certain point, where the rate of pressure recovery due to the vapour formation eventually balances and exceeds the imposed rate of decompression prior to the flashing. This point is known as flashing inception [20].

For a superheated liquid jet to remain in equilibrium after any change in the pressure condition, due to the leak, it must lose internal energy, and this is preferentially achieved through latent heat transfer. The release of latent heat of vaporization is initiated through nucleation within the liquid [14]. The critical nucleus radius at which nucleation begins is influenced by many factors and it can be estimated from a force balance on a spherical shape as:

$$r_c = \frac{2\sigma}{c_\alpha\,\Delta\mu} \tag{6}$$

where c_α is a constant. If the vapour phase can be considered as incompressible, the chemical potential can be replaced by the difference of the pressure of both phases, $p_\alpha - p_\beta$, and as result of that Eq. (6) can be written (7) [15]:

$$r_c = \frac{2\sigma}{p_\alpha - p_\beta} \tag{7}$$

The identification of the homogenous and the heterogeneous nucleation mechanisms in a jet of superheated liquid can be made using the flicker noise, $1/f$ and the fluctuation power spectrum [19,23–26]. The experimental set of data reported for Khladon-11 refrigerant (R-11) shows three different shapes of the jet originally at the saturation conditions, all as a function of the reduced temperature ratio T/T_c. The lower limit of the heterogeneous mode is determined to be located at values of $T/T_c < 0.63$, and the homogeneous region where the fluctuating production of vapour bubbles takes place and the jet shape becomes parabolic is related to $T/T_c \geq 0.90$. The intensity of nucleation in this flow mode corresponds to an explosive boiling of liquid under quasi static con-

ditions. However, it has been experimentally determined that for distances closer to the nozzle; it is possible to have liquid regions and large droplets that are still superheated. In such cases with, additionally, low rates of heat transfer in the liquid, the presence of a combination of hydrodynamic instabilities and thermal non-equilibrium conditions will then lead to the jet breaking-up into small droplets, thus giving a violent and explosive characteristic to the flashing process. On the other hand, under the same conditions but with the heat being conducted through the liquid at a sufficiently high rate, the surface evaporation takes place [11]. The equilibrium conditions for the two-phase jet will be achieved when the vapour formed from the liquid has the necessary energy to achieve equilibrium, which must be equal to the liquid phase energy [21].

4. Mechanical effects versus thermodynamic effects

Differentiating between roles of mechanical action and thermodynamic effects during the phase change processes and droplet break-up inside the jet is a complicated aspect in this study of the flashing process. A general approach that has been adopted by some authors [22] suggest that the thermodynamics part governs the process before the nozzle exit, so, the flow pattern and flow variables can be determined using theoretical model of two-phase flow as pre-existent phases, and the mechanical part will govern the spray behaviour after the nozzle exit. However, due to the intimate relationship between both mechanisms further analysis is required.

When the source pressure is increased, the flow velocity increases as a function of the square root of the difference between the pressure of the fluid inside the container and ambient pressure, there is a corresponding increase in Reynolds number. Consequently, there may be transition to turbulent regime somewhere in the supply system prior to the leak reaching the breach in containment. At higher Reynolds number, the disturbances in the liquid part of the flow are amplified involving an increase in the effects of the break-up mechanisms. Large liquid velocities at the exit of the nozzle will increase the entrainment air flow. Due to the direction of the entrained flow towards the core of the spray cone, a redistribution of the droplets inside the jet will occur.

The turbulence effects on the jet flow are important mechanical factors in the determination of the behaviour of the two-phase jet flow, once the droplets are formed. They can also promote the droplet formation on the surface of a liquid jet due to turbulent eddies presented in the flow [23] or by the influence of the turbulent instabilities on the liquid surface [24,25].The break-up mechanism inside of a two-phase jet is related to Kelvin-Helmholtz and Rayleigh-Taylor (KH-RT) instabilities [26]. Cavitation can be also considered as another mechanical process that could influence the bubble formation during flashing. The flow tendency to cavitate is proportional to the ratio of the actual pressure and vapour pressure, as well as, the kinetic energy. The flow tends to cavitate more when this ratio is increased. In the simplest cavitation models, the mass transfer is driven only by mechanical effects such as the liquid–vapour pressure differences rather than thermal effects [27].

Evaporation and boiling are the main thermodynamics processes that govern phase change during flashing. However, the developing of all of them depends on the rate of heat transfer by conduction inside the fluid, the presence of impurities and the pressure inside the flow of a given temperature. The evaporation is a superficial phase change phenomenon, in which some molecules have enough kinetic energy to escape from the liquid into the vapour state, but, due to a vapour pressure that is lower than the atmospheric pressure, bubbles of vapour cannot form. The boiling process is a volume based phenomenon, where gas bubble formation is taking place due to the vapour pressure of a liquid being equal to the local pressure (surrounding atmospheric pressure plus any hydrostatic pressure). Boiling temperature is the normal parameter used to characterize this phenomenon. Most hydrocarbon fluids have a boiling point below the standard ambient temperature. This suggests that a combination of evaporation and boiling processes can be present for this type of fluid under standard conditions. The generation of droplets over the liquid surface can also be the product of the rapid vapour bubble growth within the jet [28]. As the liquid temperature approaches boiling, the intact length and the core decreases to be replaced by a very effective atomization process. A liquid jet with low degree of superheat remains intact up to some distance from the nozzle. It is also known that for low superheat although the droplets escape from the liquid surface, the liquid column remains in the core of jet. When superheat increases the liquid column disintegrates in the early period of evaporation, after which slower evaporation of generated droplets is induced. The gradient or velocity of this decrease is also a function of the physical properties.

5. Jet characterization—post flashing process

The characterization of the flashing process resides in the information relating to the conditions inside the containment before the leak takes place, e.g., the degree of superheat of the fluid, the pressure, the properties of the fluid, the impurities present in the fluid and the internal roughness of the containment.

In realistic scenarios, it is possible to have quite accurate information about temperature, degree of superheat and the pressure of the fluid. However, the fluid properties in metastable conditions, the purity of the fluid, as well as, the nature of the exit can not be determined in the majority of the cases.

A more helpful approach is to examine the results of experiments which seek to simulate these flashing jets. The experimental approach simulates the leak using nozzles, described by parametric values or characteristics. The parameters that describe a circular nozzle are the diameter and the length. Leak paths in breaches of containment do not possess such simple symmetry. Furthermore, the actual location of the flashing point is often undetermined. It can be located inside the vessel, inside nozzle or even in some case outside of the nozzle. The flashing can be located immediately after the nozzle or some diameters after the nozzle.

The differentiation between the influences and effects of the mechanisms acting on the liquid core and on the whole jet is very complex. Combining the presence of more than one of these mechanisms in flashing, further increases the complexity of the whole problem.

It is useful to examine some aspects of the flashing jet as determined in this experimental work. Fig. 4 summarizes some of the general characteristics of a flashing jet, under the assumption that flashing occurs before or inside the nozzle, to assist in identify-

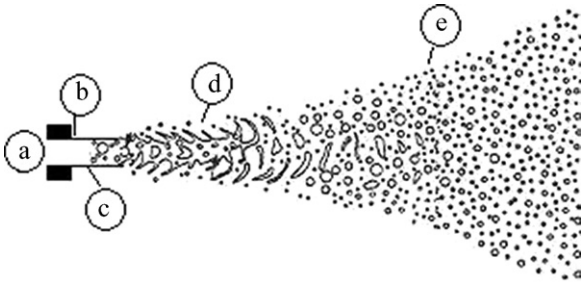

Fig. 4. Schematic flashing jet. (a) Conditions inside the vessel, (b) interface between vessel and nozzle, (c) nozzle inside path, (d) early jet zone and (e) far zone of the jet.

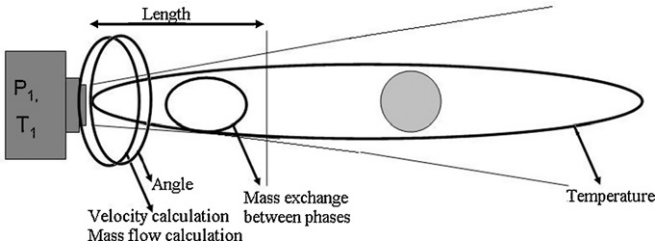

Fig. 5. Location of the variables to be calculated in the numerical approach for the flashing jet.

ing the regions where the influence of the many mechanisms has importance or can be neglected. The sections are labelled A to E and identify regions which significantly influence the overall behaviour of the flashing jet. Section A represents all the conditions inside the vessel. Section B represents the influence of the size, shape and roughness of the nozzle on the flow. Section C represents the actual path of the fluid inside the nozzle where the liquid is breaking by the bubbles already created by early nucleation. Here the boiling process is quite strong and in some cases the balance between bubble generation and the velocity of the flow through the nozzle will determine the two-phase flow pattern. In the external area of the jet, consisting of sections D and E, the surface instabilities travel outside of the nozzle, developing and breaking-up the liquid ligaments around that surface. Meanwhile, inside the jet the boiling process continues until just past section D, where there is the added complication of a phase change brought about by evaporation. After section E, the evaporation of the liquid remaining as droplets seems to be the only thermal process taking place. Here the mechanical processes such as turbulent effects, jet break-up and drag forces on the droplet together with evaporation will define the trajectory and life time of the droplet.

The numerical approaching methods currently used cover different parameters of the flashing jet that are summarized in Fig. 5. This figure identifies the parameter and the region where this parameter is calculated giving and global idea of the whole range of various equations suggested for every case to characterize a flashing jet.

5.1. Mass and velocity calculation at the exit

The calculation of the mass and the velocity at the exit of the nozzle will strongly depend on the determination of the regime of the jet at the exit of the nozzle. The regime type will determine the applicability of the calculation procedure. For instance, if the fluid remains as a superheated liquid at the outlet, then a relative large discharge rate will exist at the exit. This can be calculated with sufficient accuracy by the Bernoulli equation used to determine the flow of an incompressible fluid. However, if the flow type at the exit is described as a two-phase fluid then the flow can be estimated as a two-phase mixture in thermodynamic equilibrium or as a liquid–vapour flow in non-equilibrium according to the thermodynamic behaviour of the whole system [29].

Solomon et al. [30] described the Locally Homogeneous Flow (LHF) and the Separated Flow (SF) models, both developed to estimate the conditions after the nozzle based on the flow regime analysis. The LHF method treats the fluid as a mixture of the different fluids, with mean properties based on the individual properties of the fluids. This model is also known as homogenous equilibrium model (HEM). The SF treats the flow as a two-phase, liquid–vapour, with individual properties. Both models have, as common assumptions, the steady state condition, the one-dimensional approach, the negligible inlet kinetic energy and the absence of friction and heat transfer at the flow passage walls.

However, each model has other additional assumptions. In the case of the SF model, there are assumptions of negligible exchanges of heat, mass, and momentum between the phases, as well as, an adiabatic and frictionless expansion. Under these assumptions choked flow will exist if the pressure at exit is larger than ambient pressure and flow velocities of liquid and vapour phases can be predicted using the following expressions.

$$u_{\mathrm{l}} = \sqrt{\frac{2(p_{\mathrm{inj}} - p_{\mathrm{exit}})}{\rho_{\mathrm{l}}}} \tag{8}$$

$$u_{v} = \sqrt{2C_{p,v}(T_{\mathrm{inj}} - T_{\mathrm{exit}})} \tag{9}$$

where p_{inj} is the vessel pressure, p_{exit} is the exit pressure, ρ_{l} is the density of the fluid, $C_{p,v}$ is the specific heat coefficient of the vapour phase, T_{exit} is the exit temperature and T_{inj} is the vessel temperature.

In contrast, the LHF model assumes that the vapour and liquid have the same velocity, temperature and pressure at each cross-section. Consequently, from the energy balance, the calculation of the velocity is a function of the enthalpy difference, $h_{\mathrm{inj}} - h_{\mathrm{exit}}$, between the injection and the ambient conditions.

$$u = \sqrt{2(h_{\mathrm{inj}} - h_{\mathrm{exit}})} \tag{10}$$

Wheatley [31] reported a model for the estimation of the velocity at the discharge location, based on the constant entropy formulation during the flow path. The model covers the cases of complete liquid discharge, critical and non-critical equilibrium liquid–vapour discharges. For the pure liquid discharge, the velocity can be calculated from Eq. (8) employed by Solomon et al. [30]. For the equilibrium flow case, the discharge velocity may be calculated by Eq. (11) below. This result ignores the potential energy contribution and the loss coefficient of the nozzle.

$$u = \sqrt{2\left[\frac{(p_{\mathrm{inj}} - p_{\mathrm{exit}})}{\rho_{\mathrm{l}}} + C_{p,\mathrm{l}}(T_{\mathrm{inj}} - T_{\mathrm{exit}}) - C_{p,}T_{\mathrm{exit}}\ \ln\left(\frac{T_{\mathrm{inj}}}{T_{\mathrm{exit}}}\right)\right]} \tag{11}$$

$C_{p,\mathrm{l}}$ is the specific heat coefficient of the liquid phase. This expression may be applied to both critical and non-critical discharges. However, the thermodynamic parameters corresponding to the exit location are different in each case. For critical cases, also known as choked flow, the value of pressure at the exit will be the saturation pressure corresponding to the temperature calculated from the equilibrium expression for two-phase flow [31]. For non-critical cases, the pressure at the exit, p_{exit}, is the ambient pressure and T_{exit} is the saturation temperature at that pressure.

A report of the Fire Science Centre [32] presents a compilation of four different models of two-phase flow through a nozzle, under different assumptions. The first, the homogenous frozen model (HFM), also assumes that the vapour and the liquid have the same velocity and that the quality of the fluid through the nozzle stays constant. The enthalpy, assuming a negligible liquid contribution, can be expressed as:

$$h_{\mathrm{inj}} - h_{\mathrm{exit}} = \frac{xk}{k-1} p v_{v} \left(1 - \frac{p_{\mathrm{exit}}}{p_{\mathrm{inj}}}^{(k+1/k)}\right) \tag{12}$$

where x is the quality of the fluid in the nozzle and k is the ratio of specific heats of the fluid. The critical mass flux, G_{c}, is defined as:

$$G_{\mathrm{c}} = \frac{1}{v_{\mathrm{exit}}} \sqrt{\frac{2xk}{k-1} p v_{v} \left(1 - \frac{p_{\mathrm{exit}}}{p_{\mathrm{inj}}}^{(k+1/k)}\right)} \tag{13}$$

Under the assumption of the ratio of the specific volume of the liquid and vapour is negligibly small as given by the expression,

$(1-x)v_l/xv_v < 1$, Eq. (13) simplifies to:

$$G_c = \frac{1}{v_{exit}}\sqrt{\frac{pk}{xv_v}\left(\frac{2}{1+k}^{(k+1/k)}\right)} \quad (14)$$

The second model, which applies to fluid conditions of low quality, consists of a modification of the HFM where the effects of the liquid are only taken in the final calculation of the mass flow.

$$G_c = \frac{1}{v_{exit}}\sqrt{\frac{2xk}{k-1}pv_v(1-\eta^{(k+1/k)}) + 2p(1-x)v_l(1-\eta)} \quad (15)$$

η is the ratio of the exit pressure and internal pressure. However, in the cases where the quality approaches zero the first term of the above equation can be neglected.

The Moody's model, which is the third model in this report, assumes that the two phases are in equilibrium but do not have the same velocity. This difference in velocity is represented by a slip ratio at the exit, $SLIP_{exit}$, which is equals to $SLIP_{exit} = (u_v/u_l)\big|_{exit}$, [32]. The calculation proceeds by assuming an annular flow at the exit, then calculating the mass flow per unit area from Eq. (16) below before checking the assumption by the appropriate mass balance.

$$G_{exit} = \sqrt{\frac{2(h-h_{exit})}{(x_{exit}(v_{v,exit}(x_{exit}/\alpha_{exit}))^2 + (1-x_{exit})((1/SLIP_{exit})v_{v,exit}(x_{exit}/\alpha_{exit})))}} \quad (16)$$

The final model in this report, the Henry and Fauske model, is based on a presumption of non equilibrium flow but with liquid and vapour again possessing the same velocity. An isentropic expansion is assumed for each phase and the additional assumption is made of small heat and mass transfer between the phases. The critical mass flux is then given by:

$$G_c = \sqrt{\frac{xv_{v,exit}}{np_{exit}} + (v_{v,exit}-v_l)\frac{(1-x_{exit})N}{s_{v,exit}-s_{l,exit}}\left(\frac{ds_{l,exit}}{dp}\right) - \frac{x_{exit}Cp_{v,exit}(1/n-1/k)}{p_{exit}(s_{v,exit}-s_{l,exit})}} \quad (17)$$

n is the thermal equilibrium polytrophic exponent [32], S is the entropy of the fluid and N is defined as the partial change of quality at the throat of the nozzle. N is a function of the flow regimes and the throat pressure gradient. If $N=1$, the mass flux is close to the HEM and if $N=0$, the mass flux is close to HFM.

In another study involving an investigation into shock regime in the flow of boiling liquids through a nozzle it has been shown that, as expected, the gas fraction and the velocity discharge depend on both the nucleation before the nozzle, $J(t=0)$, and the pressure drop through the nozzle, $\wp_{12}$. The two equations for the two flow regimes as a function of the pressure drop are given below, [33].

$$u = \left[\frac{\rho_v g J(t=0) b(t=0) l^{\varsigma+1}}{(\varsigma+1)\wp_{12}}\right]^{1/\varsigma-1} \quad \text{for value of } \wp < 1 \quad (18)$$

and

$$u = \left[\frac{(\varsigma+1)^{\varsigma+2}\rho_g g J(t=0) b(t=0) l^{\varsigma+1}}{\Gamma(\varsigma+1)[\Gamma((\varsigma+2)/(\varsigma+1))]^{\varsigma+1}}\right]^{1/\varsigma-1}$$

$$\text{for value of } \wp > 1 \quad (19)$$

where l is the length of the nozzle, b is the monotonic drop in pressure, ς is the coefficient of nucleation, which equals 3 for Rayleigh phase and 1.5 for the thermal case, g is a dimensionless derivative of the nucleation, $\wp$ is the dimensionless pressure [33].

A different approach using the thermodynamic definition of jump condition was more recently introduced [34,35]. This approach establishes that at the interface between phases properties are discontinuous, but the mass, momentum and energy must be conserved. This approach also takes into account the velocity of the sound in the corresponding two-phase mixture. The general idea of this approach is highlight the relevance of the shock waves at the discharge of a superheated liquid in the jet characteristics. Numerical this is treated by the jump condition analysis. Due to the metastable liquids supply the energy stored within them via the latent heat of vaporization, the evaporation wave was assumed as an adiabatic phase transition. Additionally, it assumes the absence of work against the flow and the flow to be as isentropic. The jump conditions leaded in the Rayleigh equation and the evaporation adiabatic equation. The point where the Raleigh is tangent to the evaporation adiabatic curve, known as the lower Chapman-Jouguet point, is a unique solution to the jump condition for which the down stream condition is sonic or chocked in relation to the moving wave. However, depending on the initial thermodynamics conditions and the fluid boundary condition the subsonic flow can take place. The formulation involves a quasi one-dimensional steady evaporation wave inside the superheated liquid. The downstream condition has to be in thermal equilibrium, neglecting gravitational effects and the initial liquid condition as stagnation point. The results of this approach show that the velocities of a real discharge are closer to velocity of the sound in the fluid. Following his research line further experiments were performed using iso-octane as working fluid [36]. This new experiment setting introduces high ratios of injection to discharge pressures in flow restrictions, identifying by visualization techniques some compressible phenomena associated with the liquid flashing process from the nozzle exit section. The obtained results corroborated previous physical descriptions of flashing liquid jets, which established that flashing takes place on the surface of the liquid core through an evaporation wave process product of a sudden liquid evaporation in a discontinuous process, generating a two-phase mixture that accelerates until achieve the expansion process through a shock-wave structure. The whole system was successfully modelled and solved by numerical means using a two-dimensional axisymmetric approach. The solution was achieved by a procedure that contains two parts. The first part involves the application of the oblique evaporation waves to solve the jump formulation of the energy balance at the surface of the liquid core followed by the analysis of the expansion zone generated after this shock wave [37].

Polanco [38] using the approach of jump conditions to represent the energy, momentum and continuity equations at the inter-phase of the flashing liquid and the flashing mixture introduced the consideration of the work done in the system is equal to the resulting force at the momentum balance multiplied by the velocity of the wave. The obtained results using this new consideration have a good agreement with the experimental data reported for the cases tested.

5.2. Spray angle

A technical report from Energy Analysis INC [39] describes a method for the definition of the jet angle, β, based on the area, A_{exp}, the length, L_{exp}, of the expansion region and A, the area of the nozzle.

$$\beta = \sin^{-1}\left(\frac{A_{exp}-A}{2L_{exp}}\right) \quad (20)$$

Another definition of the spray angle is the included angle between the lines connecting the nozzle exit and the points at the spray edge at the 20 mm downstream location. The spray angle increases proportionally with the injection temperature up to certain value and then decreases. The maximum angle reported was about 82 degrees, which corresponded to the maximum pressure of 400 kPa [40]. The maximum spray angle was achieved at a dimensionless degree of superheat, $\Delta T^* = T - T_b/T_{sat} - T_b$ of between 0.45 and 0.85. This dimensionless superheat is larger than the largest

dimensionless degree of superheat previously reported by Nagai et al. [41] as 0.55.

An alternative approach to the evaluation of the spray angle, based on swirling jet data, was used by Lasheras and Hopfinger [25] and involves the growth rate, γ, of the liquid–gas shear layer. In these experiments the jet was surrounding by coaxial gas flow. This parameter is related to the ratio of liquid momentum to gas momentum, M, by the expression:

$$\gamma \approx \arctan\left(\frac{\sqrt{M}}{6}\right) \tag{21}$$

This relation only applies for values of $M < 30$ and as long as the liquid core is conical in shape. The maximum value of gamma, γ, is then about 40 degrees. However, the spray angle is larger than the liquid–gas shear layer angle (growth rate) because the inertia of the drops inside of the layer brings about further expansion of the fluid in the jet. The authors deduce from their studies that the spray angle with coaxial gas flow, α, is 45 degrees when $\sqrt{M} >> 1$. Since it is known that the liquid cone angle increases with M and that the total angle, θ, for jets into still air decreases with M from 90 to 60° approximately, the following empirical expression has been suggested for the spray angle in these circumstances.

$$\theta = 2\left(\alpha - \frac{\gamma}{2}\right) \tag{22}$$

In a separate experimental study [42] the spray angle involving coaxial gas flow for liquid cone surface is reported in as being about 50 degrees.

5.3. Mass exchange between phases

Once complete nucleation has been achieved, it is expected that the heat transfer process between the two phases takes over as the main mechanism driving the mass exchange between the phases.

The Rayleigh Plesset Model (RPM) [43] provides the basis for the determination of the mass exchange rate, $\dot{m}_{fg}$, between the liquid and the gas phases, controlling both the vapour generation and the condensation processes.

$$\dot{m}_{fg} = F\frac{3x\rho_v}{R_B}\sqrt{\frac{2}{3}\frac{|p_v - p|}{\rho_l}}\left(\frac{|p_v - p|}{p_v - p}\right) \tag{23}$$

F is a empirical factor, ρ_v is the vapour density, p_v is the vapour pressure in the bubble, p is the pressure in the liquid surrounding the bubble, R_B represents the diameter of the nucleation sites (μm) and x is the vapour volume fraction. There are two values of F for this equation, $F = 50$ for evaporation cases and $F = 0.01$ for condensation cases. A more general equation which includes vaporization is achieved by substituting for x with $x_{nuc}(1 - x)$ where x_{nuc} is the volume fraction of the nucleation sites.

Others empirical models for vapour formation have been proposed, as for instance the empirical model based on an experimental data set for propane leaking through a pipe [22].

$$\dot{m}_v = AC_D(2\rho_l(p_v - p_{pipe}))^{0.5} \tag{24}$$

where A is the area of the pipe, C_D is the discharge coefficient of the pipe, p_v is the vapour pressure inside of the pipe and p_{pipe} is the fluid pressure inside the pipe.

5.4. Flashing location/penetration

In cases where the flashing does not occur before or inside the nozzle, the exact location of the flashing corresponds to the length of the liquid core break-up. The study of this length, also called as the penetration length, has been performed in discharging liquid lies within a coaxial gas flow using an experimental technique.

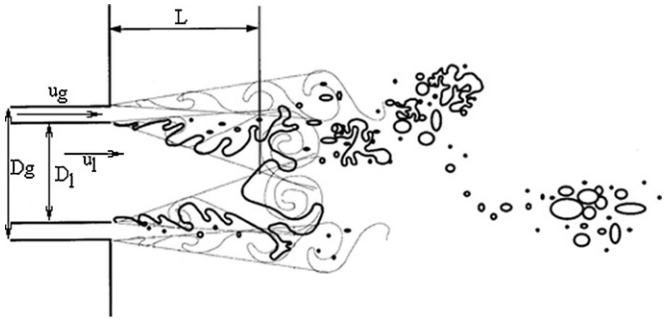

Fig. 6. Schematic representation of the liquid break-up indicating the geometry and different lengths used in the analysis.
Source: Lasheras and Hopfinger (2000).

When a liquid jet emerges from a nozzle as a continuous cylindrical shape, the cohesive and disruptive forces acting on the surface of the liquid create oscillations and perturbations. Under certain conditions the oscillations are amplified and the liquid disintegrates into droplets. This phenomenon is known as primary atomization. If the diameters of droplets exceed some critical dimension they will then disintegrate even further into smaller droplets. This process is called secondary atomization. The phenomenon of disintegration has been studied from the theoretical and experimental point of view for a very long time. A diagrammatic representation of these perturbations of the liquid surface is depicted in Fig. 6 together with the identities of some of the important parameters, such as velocity and diameters corresponding to each phase.

Lasheras and Hopfinger [25] have compiled information for such coaxial jets identifying the break-up length corresponding to different dynamics mechanisms as functions of five parameters: known as the Reynolds number, $Re = \rho uD/\mu$, the Weber number, $We = \rho_l u_l^2 D_l/\sigma$, the aerodynamic Weber number, $We_g = \rho_g u_g^2 D_g/\sigma$, the ratio of the momentum fluxes between the gas and the liquid streams, $M = \rho_g u_g^2/\rho_l u_l^2$, the gas Reynolds number, $Re_g = u_g(D_g - D_l)$, and the mass flux ratio, $m = \rho_l u_l D_l^2/\rho_g u_g D_g^2$ [25]. The core length is inversely proportional to the momentum fluxes and the Weber number.

From conservation of mass fluxes and using the capillarity wave theory, Mayer [44] obtained a direct expression for the core length as:

$$\frac{L}{D} = \frac{1}{2C_1 M^{2/3}}\left(\frac{\sigma}{\mu_l u_l}\right)^{1/3} \tag{25}$$

where C_1 is an adjustable constant. Unfortunately, this expression does not give the correct limit when the surface tension goes to zero, which coincides with the sub critical conditions of the flow. It should be noted here that there are others empirical correlations, based only on the liquid characteristic, as for instance:

$$\frac{L}{D} = C_2 We_g^{-a} Re^b \tag{26}$$

with a between 0.3 and 0.7, and b equal to 0.5.

Taking a closer look at the interaction mechanisms and presuming a dynamic pressure continuity at the liquid gas interface, the calculation of the core region length has been shown to include only the kinetic energy of the two phases [45], with exceptions for some cases where the effects of the surface tension on the actual instability formation are considerable. For these exceptional cases it is necessary to include a dynamic pressure balance at the interface [45].

In addition, the study of the instabilities of a jet emanating from a nozzle into quiescent surroundings has been performed by Lin and Reitz [46]. They considered using the length of the coherent portion of the liquid jet or its unbroken length, L, as a function

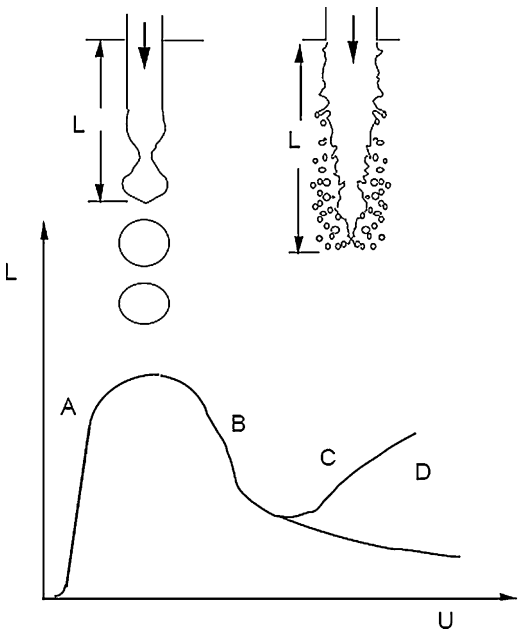

Fig. 7. Schematic diagram of the unbroken length curve. Source: Lin and Reitz (1998).

of the jet exit velocity as convenient method for categorizing jet break-up regimes. Fig. 7 shows that the unbroken length at first increases linearly with increasing jet velocity, reaches a maximum, and then decreases (regions A and B). Drops are pinched off from the end of the jet, with diameters comparable to that of the jet. There then follows a region of discontinuous behaviour of the unbroken length curve. The unbroken length increases again with increasing jet velocity (region C) and then abruptly reduces to zero (region D).

For low jet velocities (small Weber numbers) the unbroken length is proportional to the relative velocity between the jet and the gas, u_r, and inversely proportional to the maximum growth rate of the disturbance, Ω.

$$L = \frac{u_r}{12\Omega} \tag{27}$$

When the jet velocity increases the break-up mechanism is no longer produced by the capillarity pinching and it is now produced by the unstable growth of short-wavelength surface waves when the unbroken length for these cases can be expressed by:

$$\frac{L}{D} = 0.5\frac{1}{f(T)}B\sqrt{\frac{\rho_v}{\rho_l}} \tag{28}$$

where B is a constant with a typical value of 4.04 for diesel spray nozzles and $f(T)$ is a function of Taylor's parameter, T, [46].

5.5. Droplet distribution

The representation of the actual droplet size distribution is usually referred to as a frequency distribution curve. Instead of describing distributions using the location of each group of droplets with the same size or the location of each droplet with its position, there are different distribution functions based on theoretical or experimental fundamentals which show the number of droplets of a particular size. The normal distribution and the log-normal distribution are functions based on statistic principles. Alternatively, the Rosin-Rammler distribution, the Modified Rosin-Rammler and the Upper limit function are correlations based on empirical principles [13].

The Rosin-Rammler distribution is one of the functions most frequently used and it represents a probability volumetric size distribution of the drop diameters, d. This is a two parameters distribution involving a characteristic drop diameter, X, and an exponent n:

$$P = 1 - e^{-(d/X)^n} \tag{29}$$

P is the distribution defining the accumulated volume fraction of drops of diameter less than X. The characteristic drop diameter, X, is the size of a drop in the distribution whose accumulated fraction is 0.6321.

There are different characteristic diameters used to describe the mean values of the droplet distribution in various scenarios, however, the most commonly found are the Sauter Mean Diameter (SMD) and the Mean Diameter (MD). The Sauter Mean Diameter, also known as d_{32}, is the droplet diameter that has the same volume-to-surface area ratio as the total volume of all the droplets to the total surface area of all the droplets of liquid sprayed at that location. The Mean Diameter is the arithmetic mean value of the whole data set.

5.6. Temperature

The temperature distribution inside the jet in both the radial and the axial directions has rarely been reported [51–53]. At the centreline the temperature profile presents an initial decay from the exit of the nozzle until a certain distance where a minimum value is achieved, presumably connected with the location of cessation of boiling and completion of nucleation. After that point the mechanical process and the evaporation seem to be the most important mechanisms affecting the jet behaviour. This location is known as the Minimum Temperature Distance (MTD). No major observations about the value of the minimum temperature are reported in the literature. In recent experimental work carried out by Yildiz et al. [47], measurements were compared with this 1D model, [48], and good agreement was obtained between theoretical and experimental values during the first part of the temperature decay.

In comparisons of the temperature profiles at the centreline Allen [51–53] and Yildiz et al. [47] both show that propane and R134a exhibit similar thermal profile behaviours, in terms of minimum point location, for the same nozzle dimension. However, the actual value of the minimum temperature was different, about $-70\,^{\circ}C$ for propane and about $-60\,^{\circ}C$ for R134a. In general, the lateral temperature profile shows an approximately Gaussian distribution [49].

6. Modelling procedure

6.1. Introduction and general considerations

Flashing modelling has been concentrated on the study of two-phase jets behaviour under the premise that droplets are already at the inlet location together with a gas mass flux. Due to the complex of the physics involved, it is not possible to model the nucleation and boiling processes for a superheated liquid going out of containment. Therefore, the information related to the droplet formation is estimated by analytical means and after introduced to the CFD modelling as boundary conditions. These boundary conditions correspond to the liquid and gas or vapour mass flow and inlet velocity. Unfortunately, this information is not sufficient to set up a simulation. It is necessary to determine the distribution of those droplets at the inlet location. Characteristics of the droplets, as well as, their interactions with the main flow would make a difference in the modelling results. Therefore, it is quite important to understand their behaviour under certain considerations of the flow and droplets themselves, such as flow regime determined by Reynolds value, droplet sizes, interaction with turbulent structures, etc.

For low Reynolds numbers and an undisturbed flow the effects of the presence of spherical objects consists of deformation of the main flow stream lines around their bodies. This deformation will depend on the relative motion between the droplet and the mean flow. For a single object moving against the main flow, with a low relative Reynolds number, the streamlines will follow the surface of the object without any vortex shedding. If the object is moving in the same direction as the mean flow, the object movement induces flow locally so that the streamlines again lie close its surface [50].

For droplets transported by the flow, the diameter size and its comparison with the size of turbulent structure, known as eddies, could be significant in the determination of the turbulence generation or dissipation. The effect generated by the mass exchange at the surface of the droplet with the main flow and in consequence the movement of the surface due to droplet diameter changes, can generate a considerable impact in the main properties of the fluid around the droplets. If the droplets are significantly smaller than the Kolmogorov length scale (smallest turbulence scale) then the effects of the droplets can be treated as point sources in the turbulent fluid. However, if the droplets are comparable in size, or larger than, the smallest scales of turbulence, the contribution of the boundary layers on these droplets surfaces to the dynamics of the turbulent flow must be included [51]. Saffman [52] showed that the perturbation in the fluid due to the presence of a particle decays as the sum of two contributions, one as $1/r$ (long range) and the other as $1/r^3$ (short range), with r as the radius of the droplet. For droplets small compared to the smallest length scale of the flow, and for droplets separated by a distance, L, larger than their diameter, d, the most important interactions are long-range [53]. Neglecting the short range interactions, e.g., droplet wakes, is justifiable for droplets with diameters smaller than Kolmogorov's length scale of the undisturbed flow field. This justification relies on the observation that the short range perturbations are dissipated by the viscous processes.

In turbulent flow, the dispersion of the particles is controlled by the local velocity fluctuations. The velocity fluctuations produced by the particles in the fluid also affect the Reynolds stresses, either by increasing the turbulence energy or increasing the dissipation rate (turbulence modulation). Changes in Reynolds stresses affect the drag forces and the heat transfer processes between the vapour continuous phase and the dispersed phase. The small particles will attenuate the turbulence while the large particles will generate turbulence [51]. The overall reduction in turbulent kinetic energy with increasing mass loading is insensitive to the particle relaxation time; and there is a strong preferential concentration of particles into regions of low vorticity and regions with large strain rates [54,55]. Lance and Bataille [56] identified two types of non-linear coupling, the first is the stretching of the shear-induced vortices in the potential flow around the bubbles and the second is the deformation of the bubbles by these vortices, which changes the virtual volume coefficient of the bubbles and the drag force. Similarly, the liquid eddies may be deformed [57].

6.2. Modelling forces

The force in the flowing fluid is in the opposite direction to the force applied to the droplet. The forces acting on a droplet can be considered to come from three different sources. The first contribution is related with the virtual force that would have been applied to fluid element that has been displaced by the drop, i.e., the pressure forces and the viscous stresses. The second contribution is related to the perturbation of the fluid flow due to the presence of the droplets. This perturbation of the surrounding unsteady non-uniform flow results in drag, added mass and Basset history forces. The third contribution is due to the gravitational settling [52].

Elghobashi and Truesdell [58] describe the particle motion using the equations derived by Maxey and Riley [59] which treats in an independent way effects of the forces from the undisturbed flow and the disturbance to flow created by the particles. For large liquid to vapour density ratios, the particle motion was influenced by drag and gravity. The coupling between the particles and the fluid resulted in an increment of the small-scale energy. The effect of gravity resulted in an anisotropic modulation of the turbulence and an enhancement of turbulence energy level in the direction aligned with gravity. Furthermore, in the directions orthogonal to the gravity vector, the reverse cascade of energy from small to large scales was observed. Both Squires and Eaton [54] and Elghobashi and Truesdell [58] have shown that the distortion of the turbulence energy spectrum is sensitive to quantities such as the particle relaxation time. This implies that the energy transfer from the particles to the turbulence acts non-uniformly across the spectrum.

In turbulent shear flows with particles, it is often difficult to separate the direct modulation from the indirect changes in turbulence. The direct modulation is due to the fluid momentum exchange with particles. The indirect modulation is due to the modification of turbulence production mechanisms via interactions with the mean gradients of flow velocity [60]. However, for dilute flows, the authors assume that the particle motion is governed by the body forces, such as the drag, for particle relaxation times ranging between Kolmogorov's scale and Eulerian time scale and particle mass loadings up to 1 [60].

6.3. Numerical methods

Although some studies of droplet transport using Direct Numerical Simulation (DNS) have been performed [51,61]. It is important to notice that the large computational requirements of DNS restrict those studies to situation with small Reynolds numbers, whilst, the flashing process is often related with high velocities and Reynolds numbers. Therefore, due to the differences of the physics involved in each case, a direct extrapolation of the results obtained by this approach to the actual problem cannot be made.

The implementation of Large Eddy Simulation (LES) reduces the computational requirements when compared to Direct Numerical Simulation, but still requires considerable computing resources. Jin, Luo et al. [62] conducted a large eddy simulation of the two-phase plane jet to investigate the particle dispersion patterns. The particles Stokes numbers used were equal to 0.0028, 0.3, 2.5, 28 (corresponding to particle diameter 1 μm, 10 μm, 30 μm, 100 μm, respectively) in a gas flow with $Re = 11{,}300$. The particle Stokes number is defined as the ratio of the stopping distance of a particle to its characteristic dimension, $Stk = tu/d$, where t is the relaxation time of the particle, u is the gas velocity of the flow well away from the obstacle and d is the characteristic dimension of the obstacle.

Particles with Stokes numbers of 0.0028 follow the gas flow compactly. The dispersion pattern has significant differences as result of the variation of the Stokes number, particle size. The increase of Stokes numbers produce a concentration near the outer boundary of the large scale eddy structures and have nearly zero concentration throughout the central region of the structures. The simulation results of gas phase motion agreed well with previous experimental results. The simulation results of the solid particles showed that particles with different Stokes number have different spatial dispersion. The LES results are significantly more accurate than the Reynolds-averaged Navier Stokes equation (RANS) predictions of the same problem [63].

Most of the research into the modelling of turbulent particle transport has been performed using the k–ε, two equations turbulent models, as a natural extension of the single phase model, in which considerations about the generation or the dissipation of turbulence due to the presence of a second phase are incorporated [64].

Those efforts include comparison with different and more complex turbulent models. For instance, Coimbra et al. [65] compared the standard κ–ε results with the results from studies employing the multiple time scale (MTS) model for particle dispersion in turbulent multiphase mixing layers. The MTS is a four equations model that considers two ranges of turbulent energy spectrum, in the large eddy production range and in the fine-scale dissipation range. These two ranges are each associated with different time scales. On the other hand, on the basis of a two-equation turbulence model for single-phase flows, Wang et al. [66] reported the development of a pair of two-fluid turbulence models, namely, the k–ε–k_p–ε_p model and the k–ε–k_p model. These two two-fluid turbulence models show a superior performance to that of the conventional turbulence model. In a study of a gas-particle flow through a 90 degree bend using the k–ε–k_p–ε_p model, it was shown that the turbulent intensity of the particulate phase was often larger than that of the gaseous phase as would be expected from the experimental results. The model was also applied to similar flows in a vertical pipe showing good agreement with the experimental data. The k–ε–k_p model, however, uses the k–ε turbulence model for the carrier fluid and Tchen-Hinze's formula for the eddy viscosity of the particulate phase shows that the particulate turbulence intensity is always smaller than that of the gaseous phase.

The k–ε turbulent model is based on the proportionality of the turbulent kinetic energy, k, and the rate of viscous dissipation, ε, on the characteristic length scales (velocity and length). For this one-way coupling model, it is assumed that the presence of the particle phases has a negligible effect on the properties of the carrier phase. This assumption is normally valid for small particle–fluid concentration ratios or high Stokes numbers (when the particles motion is unaffected by the carrier flow field). The two-way coupled numerical method includes the effects of the particle in the carrier phase. It is worth mentioning that, due to the fact that the k–ε model is a mechanistic model, the interactions between the phases are quite easily introduced into the equations for either the one-way or the two-way coupling [64,67].

There are other types of k–ε models. For instance the Renormalised Group Theory (RNG) k–ε turbulent model produces good results from its direct application, without any modifications or inclusions, for disperse and continuous phases interaction [68], and for spray scenarios [69]. The natural way to introduce the presence of new effects on the turbulence equation model is by the definition of sources terms in the right hand side of the equation for k and ε, as follows:

$$\frac{\partial}{\partial t}(k) + (\overline{u_i})\frac{\partial}{\partial x_j}(k) = \frac{\partial}{\partial x_j}\left(\left(\nu + \frac{\varepsilon_m}{\sigma_k}\right)\frac{\partial}{\partial x_j}(k)\right) + \frac{\varepsilon_m}{\sigma_k}\left(\frac{\partial}{\partial x_j}(\overline{u_i}) + \frac{\partial}{\partial x_i}(\overline{u_j})\right)\frac{\partial}{\partial x_j}(\overline{u_i}) - \varepsilon + S_k \tag{30}$$

$$\frac{\partial}{\partial t}(\varepsilon) + (\bar{u}_j)\frac{\partial}{\partial x_j}(\varepsilon) = \frac{\partial}{\partial x_j}\left(\left(\mu + \frac{\mu_T}{\sigma_k}\right)\frac{\partial}{\partial x_j}(\varepsilon)\right) - \frac{\varepsilon}{k}\left(C_{\varepsilon 1}\overline{u_i u_j}\frac{\partial}{\partial x_j}(\overline{u_i}) + C_{\varepsilon 2}\varepsilon\right) + S_\varepsilon \tag{31}$$

Sato and Secoguchi [70] modelled the particle-induced turbulence for the bubbly flow using an enhanced continuous phase eddy viscosity, based on the introduction of a second fluctuating component that is related with all the effects generated by the droplets presence

$$\mu_t = \mu_{ts} + \mu_{tp} \tag{32}$$

where μ_{ts} is the usual shear induced eddy viscosity and μ_{tp} is an additional particle-induced eddy viscosity

$$\mu_{tp} = C_D \rho r_p \left|u_p - u\right| \tag{33}$$

where C_μ is the drag coefficient, ρ and u are, respectively, the density and velocity of the flow and r_p and u_p are the radius and velocity of the particle or droplet.

Lopez de Bertolano proposed a modification to the standard single phase κ–ε model for bubbly flow, which adds to the turbulence generated by the shear stress (SI) by introducing a new source term in the k and ε equations. In effect, this new term, S_k takes the form of and interfacial source of turbulence and implements the superimposition of the presence of the bubbles, droplets or particles on the general flow.

$$S_k = M_{ki}(u_g - u_l) \tag{34}$$

where M_{ki} is the interfacial drag force, u_g is the velocity of the gas and u_l is the velocity of the liquid. The sum of all these terms represents the work done by the gas on the liquid phase, which gets transformed into turbulent eddies.

In terms of CFD turbulence implementations, the more common model used to simulate droplet transport is the Droplet Discrete Model (DDM), which solves the equations for the continuous phase as an Eulerian flow field, and the trajectory calculation of the droplet is carried out by integrating a general force balance on a per unit particle mass basis. This approach includes in addition to the drag and gravity effects, the force required to accelerate the fluid surrounding the particle, called virtual mass force, the force due to the influence of pressure gradient, as well as the thermophoretic force due to the phenomenon known as thermophoresis. Thermophoresis is the term used to describe the phenomenon which generates forces which act in the direction opposite to the temperature gradient affecting small droplets suspended in the fluid. The method for calculating droplet collision and coalescence, based on stochastic principles involves calculation of collisions between bodies by statistical rather than deterministic methods.

Other mechanisms such as break-up and collision are also modelled. There are two general models which have been reported, the Taylor Analogy B, TAB, model and the wave model. In the TAB model the breaking requirement is given as: $x > C_b r$, where C_b is a constant equal to 0.5. The droplet breaking depends on the history of its velocity relative to the gas, which determines its distortion, instead of a unique critical Weber number which is usually used. The major limitation of the TAB model is that it only keeps track of one oscillation mode whereas in reality there are many such modes. This limitation can be attended to by using a system of a sequence of spring-mass-damped elements, one for each mode of oscillation. The TAB model is recommended for low Weber number ($We < 100$) and is well suited for low speed sprays into standard atmospheres [71,72]. The Wave Model considers the break-up of the liquid to be induced by the relative velocity between the gas and the liquid. Break-up time is determined by surface instability as a function of the wavelength and the frequency of the Kelvin-Helmholtz waves [73]. Wavelength and growth rate of these instabilities are used to predict details of the new droplets. This model is appropriate for very high velocity injection, where it is thought that the Kelvin-Helmholtz waves dominate spray break-up ($We > 100$). Hence, the wave model is recommended for Weber numbers greater than 100 at the injection points.

The simulation of jets with liquid droplets, using two commercial codes, CFX® and Star-CD®, has been reported [81,82]. The turbulence model used for the simulation was the standard k–ε model. As inlet condition for the liquid phase a Rosin Rammler distribution type was imposed, which stays downstream of the flow. The comparison of the mean value of the droplet size with the

experimental data shows a reasonable match between measurements and the calculation.

7. Review of experimental data

A general overview of the experimental work in this review has suggested a useful classification of the information into four distinct groups. The first group corresponds to the classification by the type of jet generated after the release, the second group embraces experiments involving the estimation of the droplets main diameters and droplet distributions along the jet, the third group include experiments seeking to establish velocity profiles both along the axis of the jet and in the radial direction, and the fourth group includes those experiments concerned with the temperature distribution and general thermal behaviour inside the jet. The scope of experimental data available for flashing releases of a variety of fluids including water and many hydrocarbons varies from that for very small nozzle having equivalent flow diameter in the range of 0.1–10 mm.

7.1. Type of jet generated after the release

The potential of any release to become a catastrophic event is directly related to the type of jet formed after the leakage. Unfortunately, no general model or criterion that shows clearly the effects of the mechanical and thermodynamic phenomena on this potential has been developed.

Brown and York [21] made a distinction between the three regimes of flashing for low viscosity liquids, water and R-11. These regimes are delimited by critical liquid–vapour Weber number, $We_{l,v} = \rho_v u_l^2 D/\sigma$, where ρ_v is the density of the vapour phase, d is the diameter of the nozzle, σ is surface tension and u is the velocity of the liquid phase. The first regime, for $We_{l,v} < 0.2$, is characterized by the absence of any superficial disturbances so that the only forces involved are those of interfacial tension. The second regime, for $0.2 \leq We \leq 8$, represents the break-up of jets resulting from wavelike distortions, which create perturbations of increasing magnitude leading to the disintegration of the jet into segments. The third regime, $We_{l,v} > 8$, is characterized by the presence of more violent perturbation of the jet with ligaments of fluid separating from the jet initiating the atomization process.

Peter et al. [74] observed four physical categories of flashing liquid jet for cylindrical nozzles, which they named as (a) non-shattering liquid jet, (b) partially shattering liquid jet, (c) complete shattering liquid jet involving stage-wise sequence, and (d) flare flashing liquid jet. The percentage number of smaller droplets released at the liquid break-up point increases with the increment of the superheated degree for a given ambient pressure. The mean volumetric flow-rate per unit area of the disperse jet, along the radial direction in the vicinity of its central axis, decreases with the increment in the superheated degree at constant pressure and it becomes a hollow cone with the increment in degree of superheated of the liquid. The experiments used water at temperatures between 25 and 80 °C with flashing chambers temperatures from 5 to 40 °C and an inlet water volumetric flow in the range 0.08–12 l/m depending on the nozzle involved.

Park and Lee [40] found that the internal flow pattern inside the nozzle governs the behaviour outside the nozzle. For longer nozzles or larger degrees of superheat the spray droplets are smaller and more uniform in size because of active bubble formation inside the nozzle. The flow regime changes as a response to the steady increase in superheat. The flow changes from bubbly flow to slug flow and then to annular flow. As a result, the spray droplets become smaller and more uniform, providing the basis for a classification into the three different regimes of flashing, namely a, b and c, respectively, in Fig. 8. In all these experiments, the aspect ratio (L/D) of the nozzle was about 7 and the fluid used was water. Initially, at low superheat a large intact core region is observed, and the droplets are formed at the sides of the nozzle. If the superheat is increased at the same ambient pressure, the nucleation and the growth of the bubbles become more active, so that when the bubbles collide with each other they coalesce inside the nozzle to form large slugs of liquid. When these slugs are discharged from the nozzle they break into ligaments and then disintegrate into small drops, but, exceptionally, with some of the larger ones remaining intact. In the annular flow regime, a liquid film forms on the nozzle wall and the vapour flows at a much higher velocity along the core region. In this regime, as the fluid is discharged from the nozzle, the liquid films disintegrate into fine droplets. The effect of the length of the nozzle on droplet formation is similar to that of superheat, which means that longer nozzles encourage the formation of smaller droplets outside the nozzle.

Johnson and Woodward [75] present a table with some visual observations about the type of jet achieved as a function of the pressure and the temperature using water and CFC-11 (trichlorofluorometahane) as working fluids. They find that, for a particular degree of superheat, the effect of pressure on the type of jet produced is either reduced or negligible.

Lin and Reitz [46] described the length of the coherent portion of the liquid jet as a good parameter of classification of the different jet break-up regimes, determined basically by the jet velocity but in its relation to the critical liquid-vapour Weber number, $We_{l,v} = \rho_v u_l^2 D/\sigma$, where ρ_v is the density of the vapour phase, d is the diameter of the nozzle, σ is surface tension and u is the velocity of the liquid phase. At low jet velocities, the growth of the disturbances on the liquid surface, promoted by the interaction between the liquid and gas phases, is believed to initiate the liquid break-up process. The Weber number forms the basis for the identification of for flow regimes, the first two being very similar in structure and occurring when the Weber number is less than 13. The first regime is known as the Rayleigh break-up regime, where break-up occurs many nozzle diameters downstream of the nozzle exit and droplets have larger diameters than the jet diameter. The second known as the first wind induced regime, similar to the previous one, but with droplets sizes comparable to the diameter of the jet. For high jet velocities, the break-up is due to the unstable growth of short wavelength waves on the liquid surface. The last two regimes exist at these high values of jet velocity. The third regime is the second

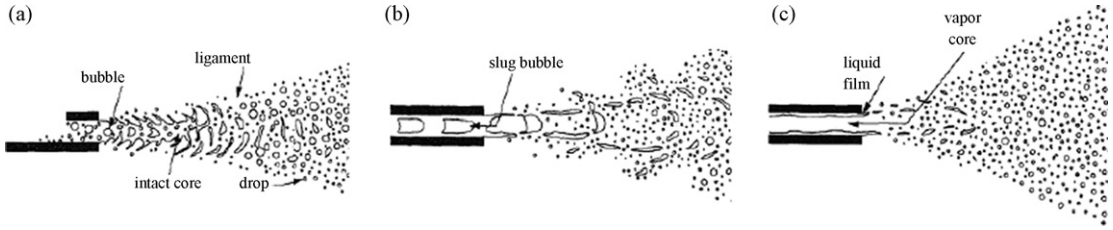

Fig. 8. Jet types dependence on nozzle (a) bubbly flow, (b) slug flow and (c) annular flow patterns.
Source: Park & Lee (1994).

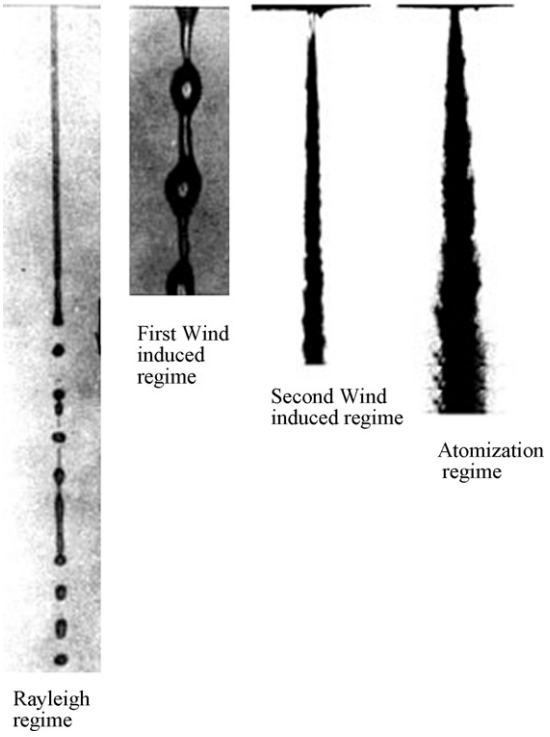

Fig. 9. Schematic jet break-up regimes: (1) Rayleigh break-up, (2) First wind induced regime, (3) Second wind induced regime and (4) Atomization regime.
Source: Lin and Reitz (1998).

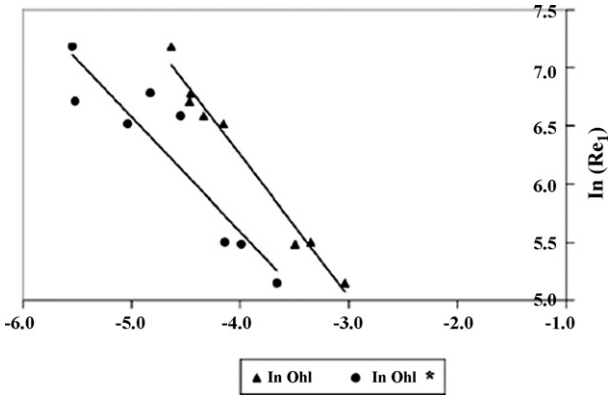

Fig. 10. The natural logarithm of Reynolds number versus the natural logarithm of Ohnesorge number and the modified Ohnesorge number calculated at the boundary between an asymmetrical jet and an atomized jet.
Source: Badens, Boutin et al. (2005).

wind induced regime, where break-up occurs some nozzle diameters downstream of the nozzle exit and the droplets have smaller diameters than the jet diameter ($13 < We_g < 40.3$). The fourth and last regime is the atomization regime, when the break-up occurs at the nozzle exit and the droplets have much smaller diameters than the jet diameter. Fig. 9 shows the different regime of the jet. They incorporated the Ohnesorge number, *Oh*, as a parameter to express the transition between regimes. The Ohnesorge number *Oh* is defined as the ratio of the viscous forces to the surface tension forces.

$$Oh_l = \frac{\mu}{\sqrt{d\rho_l\sigma}} = \frac{\sqrt{We_l}}{Re_l} \tag{35}$$

Baden et al. [76] studied the jet atomization of the fluids water, methylene chloride and ethyl alcohol into pressurized carbon dioxide at 308 K. The atomization pressure ranged from 6 to 9 MPa and the flow rate varied from 0.14 to 8.02 m s^{-1}, respectively. The results are presented in an empirical correlation for the transition boundary between the zone of the asymmetrical jet and the zone of an atomized jet as function of the jet Reynolds number, *Re*, and the Ohnesorge number, *Oh*. This correlation shows a linear relation between the logarithm of the Reynolds number and the logarithm of the Ohnesorge number and the modified Ohnesorge number, as shown in Fig. 10. The modified Ohnesorge number, Oh^*, is the original Ohnesorge number times the square root of the ratio of vapour and liquid densities.

7.2. Main droplet diameters and droplet size distributions

The second group includes those experiments which contain information relating to magnitudes of drop diameters and their distribution following leakage outside the containment. These experiments also invariably contain information relating to mass rates and the mass exchange rates between the phases. An understanding of these parameters is of considerable importance for calculations of mass flow rate and rate of mass exchange between phases as well for the implementation of numerical studies.

The majority of the authors agree on the form of the droplet size distribution in the radial direction, which is best represented as an exponential function, identified as a Rosin Rammler distribution, [53,86,87]. Many difficulties have arisen in the attempts to establish the values of the two parameters needed to define the distribution. Experiments have been performed to investigate the characteristic diameters and droplet size distribution inside two-phase jets. Some of them have achieved explicit relations for the diameter estimation based on the initial conditions of flow and presented these as size distributions [77]. It should be note that, Bayvel [78] and Fathikalajahi et al. [79] expressed doubts about the use of single value drop sizes after showing that the overall collection efficiencies were very different, depending upon whether the size distributions or a single mean diameter was employed.

Brown and York [21] reported from their observations with water and R-11 for sharp-edged and rough surface orifices that, at a location 6 inches (0.15 m) downstream from the nozzle, a linear correlation exists between the temperature and the mean diameter, which implies a inverse proportionality between the MD and the Weber number of the fluid.

Solomon et al. [30] performed an experimental study on a flashing injector using two different fluids: the fuel named Jet-A containing dissolved air and pure R-11. A two stage expansion process was used, separated by an expansion chamber, which was found to be beneficial for good atomization of the jet. The mass flow, the mass velocity, the spray angle, as well as the Sauter mean diameter as functions of the pressure and the axial distance were reported. These results are compared with the predictions from Local Homogeneous Flow and Separated Flow models.

Nagai et al. [41] studied the atomization of the superheated liquid jet using water as the working fluid. A dependency of the bubble generation on the resident times inside the nozzle and, therefore, on the length of the nozzle and the velocity of the fluid was reported. In this work the dimensionless degree of superheat of the fluid was defined as the ratio between the degree of superheat and the difference between the saturation temperatures at the injection pressure and at the ambient pressure, taken as 100 °C. The Reynolds number times the aspect ratio, *L*/*D*, of the nozzle identified the type of atomization of the jet as either liquid column break-up or two-phase flow. A set of equations for the calculation of the SMD based on the dimensionless degree of superheat of the fluid, the Reynolds and the length diameter ratio of the nozzle is given.

Wheatley [31] developed an expression, involving the Weber number and the Reynolds number of the jet, which predicts the maximum drop size, taking into account the implications of the effects of rain-out processes.

Hervieu and Veneau [80] made experimental determinations of the droplet sizes within a jet at the exit of a discharge pipe of a liquefied propane storage tank during a sudden blow down. A series of blow down experiments was performed varying the nozzle diameter (2, 5 and 8 mm), the initial pressure (5, 11 and 17 bar). The volume of the tank was 5 l and half filled with propane liquid. The diameter of the jet at a location 60 mm downstream from the nozzle was determined for different nozzle sizes at 11 bar initial pressure, in one series of experiments, and for a 2 mm nozzle at the three different pressures in another series. The mean droplet diameter always remained constant during the total liquid release, and for all the cases the flat shape of the diameter-velocity cross-correlation curve indicated that droplets of each size group were moving with the same velocity. In addition, it was shown that the diameters and velocities decrease in the radial direction. This finding was taken to confirm that the evaporation process develops, predominantly, in the flow direction. Measurements of the droplet size and velocity at 95 mm from the nozzle were also recorded.

Gemci et al. [27] made parametric studies of a feed of a binary mixture of water and acetone with nitrogen as propellant gas. They found that the presence of the flashing fluid can markedly reduce the amount of propellant gas required for the same mean droplet diameter.

Deaves [81] used an empirical correlation, based on data for sprays formed from the flow of fluids through orifices to calculate the SMD, required as input for CFD modelling of clouds formed after an accidental release. The drag coefficient was assumed to be a function of the droplet diameter and it could be related to the rate of reduction of the droplet diameter. The study defined a criterion to determine those droplets which evaporate completely during the turbulent decay phase, and which drops only reduce in size.

Yildiz et al. [52,55,90] carried out experimental research on a flashing jet of R134a jet using Global Rainbow Thermometry (GRT), Phase Doppler Anemometry (PDA) and Particle Image Velocimetry (PIV) techniques. This investigation reported the SMD and the MD distribution on the centreline, the temperature profile and the velocity field distribution on the centreline and also at two different radial positions ($x/d = 187$ and $x/d = 507$). In addition, images of the jet behaviour were recorded. The droplet size evolution along the jet axis shows the presence of expansion and entrainment regions. Also in the axial direction, the larger droplets were found to be, as expected, located near the centreline of the jet. Measurements were made within a matrix of three distinct ambient pressures (8.2, 8.86 and 9.42 bar), three distinct degrees of superheat (43.4, 47.9 and 49.6 °C) and two nozzles sizes (1 and 2 mm). An increase in the diameter of the nozzle was found to be associated with the more violent break-up processes and with a decrease in the disintegration distance from the nozzle. The degree of superheat has a direct effect on the number of bubbles generated, because this parameter reflects the level of energy available from the liquid. So, for larger superheat values more energy is released and more droplets are generated and a complete shattering of the jet takes place inside the nozzle.

Gemci et al. [82] studied the flash atomization of water/acetone solutions with a propellant gas by varying three operating variables, namely, the relative concentration of the propellant gas and the liquid, the injection temperature, and the pressure. These studies were extended by Gemci et al. [27] with solutions of different concentrations of binary mixtures of n-hexadecane and n-butane (2 and 5 wt% n-butane in hexane), employing nitrogen as the propellant gas. The mean droplet diameters were measured as a function of the injection temperature, the pressure, and the nitrogen-to-liquid flow rate ratio. The quantity of liquid present improves the atomization under all conditions, whereas the quantity of gas propellant increases the injection velocity and promotes bubble formation. Both, temperature and pressure enhance the atomization process. A stronger effect in relation to these changes as functions of propellant gas rate were reported for water alone when compared with the acetone/water solutions. This effect was correlated on the basis of linear relationships between the SMD and both the dimensionless superheat temperature difference, ΔT^*, and the cavitation number, K, when measurements were recorded 3 cm downstream from the nozzle.

It has been noted that large droplets predominate in the core region of swirling jets. Madsen et al. [83] reported the droplets size measurement, using interferometry particle imaging (IPI) and Doppler PDA measurement, for a Danfoss oil pressure-swirl atomiser operated with a flow rate approximately of 3.2 l/h of water, corresponding to an atomization pressure of 850 kPa. The results obtained by these two methods were similar, with the PDA results consistently recording larger droplets than those for IPI. The range of droplet diameters was found to lie between a maximum of 70 μm and a minimum of 20 μm. Additionally, Takeuchi et al. [84] reported the measurement of the MD and the SMD of a water spray centrally injected through a 10 mm diameter nozzle into a swirling annular jet of 56.5 mm diameter entry, with both heated and non-heated airflows. Both the SMD and the MD decrease in the radial direction from the centreline towards the edge of the spray. As expected, the MD was smaller for the heated case due evaporation, even in axial directions some distance from the nozzle centreline.

7.3. Velocity profiles

In experiments into flashing jets involving propane, Allen [6,53,94–96] reported results for the axial propane droplet velocity and relative volumes by size range, as a function of the radial distance from the centreline. Nozzles of 4 and 6 mm diameter were used. These parameters were presented along the measurement lines at axial position of 0.500, 0.688 and 1.088 m, as well as, along the centreline. The two ranges are 0–21.4 μm and 21.4–41.2 μm. The centreline measurements show an initial reduction in the relative fraction of both size bands from locations 0.5 to 1 m downstream of the nozzle, followed by an increase at larger distances, possibly, due to coalescence, or the effects of rates of evaporation varying with droplet size. No observations were made regarding the jet shapes. The first part of the centreline axial velocity is approximately constant, and then it starts decreasing in the axial direction with distance from the nozzle. The exit velocity was estimated to be around 30 m/s (core section) and the average mass release rate for 4 mm nozzles was 0.11 kg/s with a standard deviation of 0.02 kg/s. The radial velocity profile at different positions has a Gaussian shape, as expected. The dimensionless plot of these profiles suggests that the jet spreads at a constant rate. Cases using R-22 as fluid with 2.8 and 1 mm pinholes showed similar results.

Mcdonnel [85,86] studied the flashing process for methane. The expansion of the velocity profile for methane indicates that the jet angle close to the nozzle is large but not as large as corresponding jet angles for propane. The radial velocity profile showed a Gaussian shape. Axial velocity profiles were not reported. However, axial velocity profiles can be inferred from the radial distributions, which show that all the measurements were made in the decay region of the jet.

Vieira and Simões-Moreira [36] performed a campaign of experiments using iso-octane as working fluid. They used visualization techniques to characterize the whole flashing process for flashing liquid discharges at very high ratios of injection into a low-pressure chamber. The used visualization techniques were the Schlieren and the back-lighting methods. They could identify the compressible

phenomena associated with the liquid flashing process from the nozzle exit section. Images of the shock-wave structure in the phase change region around the liquid core were taken using the Schlieren method in conjunction with the observation of the central liquid core of the jet reaches by the application of the back-lighting optical technique. The obtained results actually show that the phase change occurs under the presence of a shock wave structure, where the liquid evaporates suddenly following a discontinuous process, but once the two-phase mixture appears it accelerate up to sonic speed that characterize the critical condition of the compressible flow and limit the maximum mass flow of the whole system. The critical condition corresponds to the Chapman–Jouguet condition. After this point the mixture follows its acceleration achieving a supersonic condition required to produce a shock wave. They also proposed a numerical model that was successfully compared with the experimental values obtained [37].

7.4. Thermal behaviour

This, the fourth group of experimental results concerns the temperature characteristic of the flashing jet. It involves the time dependent relationships of jet temperature, as well as, the behaviour of the temperature profile along the centreline and in the radial direction.

Miyatake et al. [87,88] made an experimental study of spray flash evaporation in superheated water injected through a circular tube nozzle into a low-pressure vapour zone. The inlet temperature was 40, 60 or 80 °C. The glass nozzles used had internal diameters of 0.346, 0.502 and 0.815 cm, with lengths of 12, 25 and 25 cm, respectively. The time dependent temperature profile at the centreline of the spray flash shows two exponential decaying processes expressed as

$$\theta = e^{-s_1(t-t_o)} \quad t_o \le t \le t_i \tag{36}$$

$$\theta = e^{-s_2(t-t_o)} \quad t_i \le t \tag{37}$$

where θ is the dimensionless temperature of liquid in the centre of the jet, defined as $\theta = (T - T_{sat}(p_v))/(T_o - T_{sat}(p_v))$, t_0 is the time lag of the initiation of flashing and t_i are the values of the interception of the two functions.

The temperature profile along the centre line shown by Allen [89], suggests that the Minimum Temperature Distances (see Section 5.6 of this review) measured correspond to the limit of droplet existence, at 0.66 m. The measured temperature at this location was −70 °C. After this point there is a rapid rise in temperatures to 25 °C in 0.1 m. Temperatures continue to rise downstream, though the rate of increase diminishes. It is believed that the MTD for any release will be between $x/D = 150$ and $x/D = 170$ [89].

For the same diameter of discharge nozzle of 4 mm, experimental data from studies by MTD of R134a, Yildiz et al. [47], with similar values of MTD exhibit the same thermal profile behaviours as the data reported by Allen [89]. Although the minimum temperature was about −60 °C, different to that for propane, the gap between the minimum temperature and the boiling point of each fluid was about 30 degrees. Moreover, for different nozzle diameters the MTD increases but the temperature gap stays constant [90].

8. Summary and concluding remarks

The state of our knowledge about flashing jet phenomena as revealed in this review suggests that there is still a long way to go before we can predict with any confidence how such jets will behave in any situation. Hence, we cannot, at this time, provide guidance as to how the consequences of losses of containment of superheated liquids can be controlled or their affects mitigated except in some very limited cases.

It is therefore our intention, in this section, to identify the shortfall in our knowledge by way of four areas as follows (a) controlling phenomena—thermal and mechanical; (b) jet behaviour viewed in terms of the most significant jet parameters; (c) data available from experimental studies; and (d) the ability to predict flashing jet behaviour by theoretical models or numerical procedures.

8.1. Controlling phenomena—thermal and mechanical

Both mechanical and thermodynamic processes are involved. It appears that for the first region of the jet, the expansion region, it is the thermodynamic processes which dominate. It is only after the flashing point, where the internal pressure of the jet becomes equal to the atmospheric value and the jet enters the entrainment region, that the mechanical processes become dominant. The potential danger level of a release is a function of the calculated values of the mass flow. These have a strong dependence upon the way in which nucleation and energy release in jet expansion are modelled. Hence, it is essential that we develop a real understanding of the interaction of the mechanical and thermal processes.

8.2. Jet behaviour viewed in terms of the most significant jet parameters

8.2.1. Superheat and pressure

Jet flashing behaviour is very sensitive to small changes in the degree of superheat and to a lesser degree with respect to pressure variations. However, the nature of the final discharge – superheated liquid or an atomized jet – will depend on a combination of pressure, temperature and the geometry of the nozzle. This dependency is not well understood yet [13,52,55,90,100].

8.2.2. Jet angle

It is expected that the droplet size, its size distribution and its relative velocity to the continuous phase will affect the jet angles and the length of the core region. Dense droplet concentrations increase the jet angle, as do large relative velocities. The jet angle depends on the level of violence of the flashing process at the nozzle exit, with the more violent phase changes producing larger angles. However, existing correlations for jet angles do not take account of the type of jet created after the leak.

8.2.3. Droplet size and distribution

Droplet distribution can be represented as a symmetrical function without major errors, as for instance the Rosin Rammler distribution. Furthermore, the almost constant value of the Sauter Mean Diameter along to the jet axis suggests that heat conduction, evaporation, the rate of break-up and turbulence are balanced along the jet axis, [80].

8.2.4. Jet temperatures

The Minimum Temperature Distance is an important parameter defining the end of the boiling and nucleation process, and the start of the mechanical processes. It should be noted that evaporation still plays an important part in the jet behaviour after this point. The temperature profile at the centreline consists of an initial decay of the temperature, possibly to below the boiling point, followed by a recovery to the ambient further downstream. The radial profile of temperature follows a Gaussian shape [51–55].

8.3. Data available from experimental studies

There are number of problems associated with the various experiments for which data is available making it very difficult to categorize the locations of this information.

For instance, the detailed circumstances for the tests are often not reported fully and on other occasions unusual materials or mixtures of materials have been used. However, we can make a very short summary of existing experimental work related to a few specific jet parameters or characteristics. Thus, for type of jet generated, we have the work of Badens et al., Brown and York, Hayashi et al., Lin and Reitz, Park and Lee and Peter et al. [27,43,49,83–85], for velocity we have the work of Allen and McDonell et al. [53,94–98], in the matter of droplet sizes we have the work of Brown and York, Gemci et al., Madsen et al., Nagai at al., Solomon et al., Takeuchi et al. and Yildiz et al., [27,33,36,44,55,90–93], and regarding temperature we have the work of Allen, Miyatake et al. and Yildiz et al. [51–53,99]. Finally, for mass flow at various locations in the jet we have the work of the Energy Analysts INC [39].

8.4. The ability to predict flashing jet behaviour by theoretical models or numerical procedures

Existing models that describe the type of jet are concerned with the identification of the different types of jet, [27,43,49,83–85]. No complete qualitative or quantitative model is available to determine the type of jet generated after the leak. It is very hard to establish any correspondence between two or more different criteria for describing the different regimes based on dimensionless numbers (Reynolds Number, Weber Number, Ohnesorge Number, Jacob number, the nozzle aspect ratio, dimensionless degree of superheat) [27,43,49,83–85]. A comprehensive model to evaluate the final state of the fluid in a flashing jet that includes pressure and temperature effects, as well as, the geometric complexity is still to be discovered. Approximate calculations of the liquid and gas mass discharge rates and the diameter of droplets in the downstream region of the jet may be made using empirical equations or, under certain theoretical assumptions, using analytical solutions of the basic equations [35–39]. Comparing a few models, the Separated Flow model overestimates the velocity, the values given by Locally Homogeneous Flow, which is based on the same velocity for gas and liquid phases, appear to be more realistic. Furthermore, the results obtained by Locally Homogeneous Flow model compare even better with the experimental data [30,91]. Amongst the other models, the Henry and Fauske model does not yield the expected values for isentropic or isothermal cases [32] and the shock regime formulae for flow of boiling liquids trough a nozzle requires the difficult task of determining nucleation characteristics of the flow before it reaches the nozzle making this technique unusable in all practical situations [33].Numerical modelling of two-phase jets with various turbulence models has been successfully employed. It has been shown that k–ε model types are preferred due to their relatively simplicity with respect to others turbulence models. Comparison of complete CFD simulations using the k–ε model show good agreement with the experimental data in the far region of the velocity decay [91,92].

Different authors have studied the direct applicability of the k–ε turbulent model to two-phase flow cases, [74,75], as well as its applicability after the definition of sources terms in the right hand side of the equation of k [70,93]. These source terms have the diffusive form, which include the second gradient of the velocity field and the relative velocity is recognized as an important parameter with respect to the new definitions for droplet viscosity. These hypotheses try to compensate for the effect of the main assumptions in the model relating to the isotropic and homogenous characteristic of the turbulence.

References

[1] N.T.S. Board, Hazardous Materials Accident Summary Report Failure of Tank Car TEAX 3417 and Subsequent Release of Liquefied Petroleum Gas, Pasadena, Texas, November 22, 1997, Washington, D.C., 1998.
[2] N.T.S. Board, Hazardous Materials Accident Brief, Washington, D.C., 1998.
[3] N.T.S. Board, Railroad Accident Report, Derailment of Union Pacific Railroad Train QFPLI-26 at Eunice, Louisiana, May 7, 2000, Washington, D.C., 2002.
[4] J.T. Allen, Laser-based Droplet Size Measurements in Two-phase, Flashing Propane Jets, Health and Safety Laboratory, 1996.
[5] G.N. Abramovich, The Theory of Turbulent Jets, The M.I.T Press, USA, 1963.
[6] B.A.F. Simpson, A computational study of gas leak jets relevant to offshore structures, in: Aeronautical, Civil and Mechanical Engineering, University of Hertfordshire, Hatfield, 1998.
[7] S.J. Wakes, A.E. Holdo, A.J. Meares, Experimental investigation of the effect orifice shape and fluid pressure has on high aspect ratio, Journal of Hazardous Materials A89 (2002) 1–27.
[8] B.S. Massey, Mechanics of Fluids, sixth ed., Chapman & Hall, London, 1989, p. 599.
[9] B.J. Hill, Measurement of local entrainment rate in the initial region of axisymmetric turbulent air jet, Journal of Fluid Mechanics 51 (4) (1972) 773–779.
[10] H.W. Liepman, J. Laufer, Investigations of Free Turbulent Mixing, in NACA TN 1257, National Advisory Committee for Aeronautics, Washington, 1947.
[11] D. Yildiz, Dynamics of Two-phase Flashing Jets. VKI Lectures Series, von Karman Institute for Fluid Dynamic, Belgium, 2003.
[12] G.J. Van-Wylen, R.E. Sonntag, C. Borgnakke, Fundamentals of Classical Thermodynamics, ed. I, Jonh Wiley & Sons, New York, 1994.
[13] A.H. Lefebvre, Atomization and Sprays, Hemisphere Publishing Corporation, USA, 1989.
[14] P. Whalley, Boiling, Condensation and Two-phase Flow, Oxford University Press, London, 1979.
[15] J.M.P. Schmelzer, Kinetic and thermodynamic theories of nucleation, Materials Physics and Mechanics 6 (2003) 21–33.
[16] M. Das, et al., How high can the temperature of a liquid be raised without boiling? Physical Review E 62 (4) (2000).
[17] C. Frederic, S. Balibar, H.J. Maris, Limit of metastability of liquid helium, Physica B 329–333 (1) (2003) 356–359.
[18] A.V. Reshetnikov, et al., 1/f Fluctuations in critical modes of flow of superheated liquid, Heat and Mass Transfer and Physical Gas Dynamics 40 (3) (2002) 443–446.
[19] B. Christensen, M.S. Tillack, Survey of Mechanisms for Liquid Droplets Ejection from Surfaces Exposed to Rapid Pulsed Heating, in UCSD-ENG-100, Fusion Division, Center for Energy Research, University of California, La Jolla, CA, 2003.
[20] E. Elias, P.L. Chambre, Flashing inception in water during rapid decompression, Journal of Heat Transfer 115 (1993) 231–238.
[21] R. Brown, L. York, Sprays formed by flashing jets, American Institute of Chemical Engineers 8 (2) (1962) 149–153.
[22] M.A. Aamir, A.P. Watkins, Numerical analysis of depressurisation of highly pressurised liquid propane, International Journal of Heat and Fluid Flow 21 (2000) 420–431.
[23] P.K. Wu, L.K. Tseng, M. Faeth, Primary breakup in gas/liquid mixing layers for turbulent liquids, Atomatization and Sprays 2 (1992) 295–317.
[24] P. Bricard, L. Friedel, Two-phase jet dispersion, Journal of Hazardous Materials 59 (1998) 287–310.
[25] J.C. Lasheras, E.J. Hopfinger, Liquid jet instability and atomisation in coaxial gas stream, Annual Review Fluid Mechanics 32 (2000) 275–308.
[26] C.S. Lee, S.W. Park, A numerical study on fuel atomization characteristics of high-pressure diesel injection sprays, Fuel 81 (2002) 2417–2423.
[27] T. Gemci, et al., Flash atomization of water/acetone solutions, Atomization and Sprays 14 (2004) 459–475.
[28] R.D. Reitz, A photographic study of flashing-boiling atomization, Aerosol, Science and Technology 12 (1990) 561–569.
[29] S. Khajehnajafi, A. Shinde, Prediction of discharge rate from pressurized vessel blowdown through sheared pipe, Process Safety Progress 13 (2) (1994) 75–82.
[30] Solomon, et al., Flow and atomization in flashing injectors, Atomization Spray Technology 1 (1985) 53–76.
[31] C.J. Wheatley, A Theoretical Study of NH3 Concentration in Moist Air Arising From Accidental Releases of Liquefied NH_3, Using the Computer Code TRAUMA, Health and Safety Executive, 1987.
[32] Fire_Science_Centre, The Blowdown of Pressurized Containers, Fire Science Centre, University of New Bruswick, 1994.
[33] V.P. Skripov, et al., Thermophysical Properties of Liquids in Metaestable (superheated) State, Gordon and Breach Science Publisher, Amsterdam, 1988.
[34] J.R. Simões-Moreira, Oblique evaporation waves, Shock Waves 10 (2000) 229–234.
[35] J.R. Simões-Moreira, C.W. Bullard, Pressure drop and flashing mechanisms in refrigerant expansion devices, International Journal of Refrigeration 26 (2003) 840–848.
[36] M.M. Vieira, J.R. Simões-Moreira, Low-pressure flashing mechanisms in isooctane liquid jets, Journal of Fluid Mechanics 572 (2007) 121–144.
[37] E. Angelo, J.R. Simões-Moreira, Numerical solution of highly expanded flashing liquid jets, Journal of Thermophysics and Heat Transfer 21 (2) (2007) 379–391.
[38] G. Polanco, Phase Change Within Flows from Breaches of Liquefied Gas Pipelines, Coventry, Coventry, 2008.
[39] Energy_Analysts_INC, Release characteristics of superheated water and FC-11 liquids an experimental program, 1990.
[40] B.S. Park, S.Y. Lee, An experimental investigation of the flash atomization mechanism, Atomatization and Sprays 4 (1994) 159–179.
[41] N. Nagai, K. Sato, C.W. Lee, Atomisation characteristics of superheated liquid jets, in: ICLASS-85, International Conference on Liquid Atomisation and Spray System, Imperial College, London, 1985.

[42] L. Raynal, E. Villermaux, E.J. Hopfinger, Primary instability of a plane liquid-gas shear layer, Journal of Fluid Mechanics (1999).
[43] T. Giese, E. Laurien, A three dimensional numerical model for the analysis of pipe flows with cavitation, in: Nuclear technology 2000, Bonn, 2000.
[44] E. Mayer, Theory of liquid atomization in high velocity gas streams, ARS 31 (12) (1961) 1783–1785.
[45] H. Rehab, E. Villermaux, E.J. Hopfinger, Flow regimes of large velocity ratio coaxial jets, Journal of Fluid Mechanics 345 (1997) 357–381.
[46] S.P. Lin, R.D. Reitz, Drop and spray formation from liquid jet, Annual Review Fluid Mechanics 30 (1998) 85–105.
[47] D. Yildiz, J.P.A.J.v. Beek, M.L. Riethmuller, Global rainbow thermometry applied to a flashing two-phase R134-A Jet, in: 11th International Symposium on Application of Laser Techniques to Fluid Mechanics, Lisbon, Portugal, 2002.
[48] H. Pretrel, Etude du comportemnet thermohydrauliquie de pulverisation liquies sous l'effet d'un rayonnement infrarouge application a la protection incendie par rideau d'eau, in Ecole Doctorale des Sciences de L'Inegenieur de Lyon, M.E.G.A., 1997, L'Institut National des Sciences Appliquees de Lyon, Lyon, p. 280.
[49] D. Yildiz, P. Rambaud, J.V. Beek, Break-up, droplet size and velocity characterisation of a two-phase flashing R134A jet, in: 5th International Conference on Multiphase Flow, Yokohama, Japan, 2004.
[50] J. Happel, H. Brenner, Low Reynolds Number Hydrodynamics, Martinus Nijhoff Publishers, The Hague, 1983.
[51] Crowe, Troutt, Chung, Numerical models for two-phase turbulent flows, Annual Reviews 28 (1996) 11–43.
[52] P.G. Saffman, On the settling speed of free and fixed suspension, Studies in Applied Mathematics 52 (1973) 115–127.
[53] D. Koch, Kinetic theory for a monodisperse gas-solid suspension, Physics Fluids A 2 (1990) 1711–1723.
[54] K.D. Squires, J.K. Eaton, Particle response and turbulence modification in isotropic turbulence, Physical Fluids A 2 (1191) (1990).
[55] L.P. Wang, M.R. Maxey, Settling velocity and concentration distribution of heavy particles in homogeneous isotropic turbulence, Journal of Fluid Mechanics 256 (27) (1993).
[56] M. Lance, J. Bataille, Turbulence in the liquid phase of a uniform bubbly air-water flow, Fluid Mechanics 22 (1991) 95–118.
[57] I. Kataoka, A. Serizawa, Basic equations of turbulence in gas-liquid two-phase flow, International Journal of Multiphase Flow 15 (5) (1989) 843–855.
[58] S.E. Elghobashi, G.C. Truesdell, On the two-way interaction between homogeneous turbulence and dispersed solid particles. I: Turbulence modification, Physics Fluids A 5 (1790) (1993).
[59] M.R. Maxey, J.J. Riley, Equation of motion for a small rigid sphere in a nonuniform flow, Physics Fluids 26 (4) (1983) 883–889.
[60] M. Boivin, O. Simonin, K.D. Squires, Direct numerical simulation by particles in isotropic turbulence, Journal of Fluid Mechanics 375 (1998) 235–263.
[61] F. Mashayek, Droplet turbulence iterations in low mach number homogeneous shear two-phase flows, Fluid Mechanics 367 (1998) 163–203.
[62] H.H. Jin, et al., Large eddy simulation of a particle-laden turbulent plane jet, Journal of Zhejiang University Science 4 (2) (2003) 175–180.
[63] S.V. Apte, et al., Large eddy simulation of swirling particle laden flows in a coaxial-jet combustor, International Journal of Multiphase Flow 29 (2003) 1311–1331.
[64] S.L. Lee, J.R.T. Lahey, J.O.C. Jones, The prediction of two-phase turbulence and phase distribution phenomena using a k-e model, Journal of Multiphase Flow 3 (1989) 335–368.
[65] C.F.M. Coimbra, J.S. Shirolkar, M. Queiroz McQuay, Modeling particle dispersion in a turbulent, multiphase mixing layer, Journal of Wind Engineering and Industrial Aerodynamics 73 (1) (1998) 79–97.
[66] Y. Kang, S. Komori, A two-fluid turbulence model for gas-solid two-phase flows, Journal of Chemical Engineering of Japan 30 (3) (1997) 526–534.
[67] C.S. Lee, S.W. Park, An experimental and numerical study on fuel atomization characteristics on high-pressure diesel injection sprays, Fuel 81 (2002) 2417–2423.
[68] R. Andersson, et al., Development of a multi-scale simulation method for design of novel multiphase reactors, Chemical Engineering Science ISCRE18 59 (22–23) (2004) 4911–4917.
[69] L.X. Huang, K. Kumar, A.S. Mujumdar, A comparative study of a spray dryer with rotary disc atomizer and pressure nozzle using computational fluid dynamic simulations, Chemical Engineering and Processing 45 (6) (2006) 461–470.
[70] Y. Sato, K. Secoguchi, Liquid velocity distribution in two-phase bubble flow, International Journal of Multiphase Flow 2 (1975) 79–95.
[71] P.J. O'Rourke, Collective Drop Effects on Vaporizing Liquid Sprays, Princeton University, Princeton, New Jersey, 1981.
[72] P.J. O'Rourke, A.A. Amsden, The TAB method for numerical calculation of spray droplet breakup. SAE Technical Paper 872089, SAE, 1987.
[73] R.D. Reitz, Mechanisms of breakup of round liquid jets, The Encyclopedia of Fluid Mechanics 3 (1986) 223–249.
[74] E.M. Peter, A. Takimoto, Y. Hayashi, Flashing and shattering phenomena of superheated liquid jets, JSME International Journal 37 (2) (1994) 313–321.
[75] D.W. Johnson, J.L. Woodward, RELEASE A Model with Data to Predict Aerosol Rainout in Accidental Releases, Center for Chemical Process Safety, American Institute of Chemical Engineers, New York, 1999.
[76] E. Badens, O. Boutin, G. Charbit, Laminar jet dispersion and jet atomization in pressurized carbon dioxide, The Journal of Supercritical Fluids 36 (2005) 81–90.
[77] M.A.M. Costa, et al., Droplet size in a rectangular Venturi scrubber, Brazilian Journal Chemical Engineering 21 (2) (2004).
[78] L.P. Bayvel, The effect of polydispersity of drops and the efficiency of a Venturi Scrubber, Transaction of the Institution of Chemical Engineering 60 (1982) 31–34.
[79] J. Fathikalajahi, M.R. Talaie, M. Taheri, Theoretical study of nonuniform droplets concentration distribution on Venturi crubber performance, Particulate Science and Technology 14 (1996) 153–164.
[80] H. Hervieu, T. Veneau, Experimental determination of the droplet size and velocity distributions at the exit of the bottom discharge pipe of a liquefied propane storage tank during a sudden, Journal of Loss Prevention in the Process Industries 9 (6) (1996) 413–425.
[81] D.M. Deaves, et al., Modelling of catastrophic flashing releases, Journal of Hazardous Materials A88 (2001) 1–32.
[82] T. Gemci, et al., Experimental study of flash atomization of binary hydrocarbon liquid, International Journal of Multiphase Flow 30 (2004) 395–417.
[83] F. Madsen, et al., Measurement of droplet size and velocity distributions sprays using interferometric particle imaging (IPI) and particle tracking velocimetry (PTV), in: ICLASS 2003, Sorrento, Italy, 2003.
[84] G. Takeuchi, et al., Spatial distributions of droplet size and velocity in air heated spray measured by interferometric laser imaging technique, in: 12th International Symposium Applications of Laser Techniques to Fluid Mechanics, Lisbon, Portugal, 2004.
[85] V.G. McDonell, M. Adachi, G.S. Samuelsen, Structure of reacting and nonreacting, nonswirling, air-assisted sprays. Part I: gas-phase properties, Atomatization and Sprays 3 (1993) 389–410.
[86] V.G. McDonell, G.S. Samuelsen, An experimental data base for the computational fluid dynamics of reacting and nonreacting methanol sprays, Journal of Fluids Engineering 117 (1995) 145–153.
[87] O. Miyatake, et al., An experimental study of spray flash evaporation, Desalination 36 (2) (1981) 113–128.
[88] O. Miyatake, et al., Effect of liquid temperature on spray flash evaporation, Desalination 37 (3) (1981) 351–366.
[89] J.T. Allen, Laser-based Measurements in Two-Phase Flashing Propane Jets, University of Sheffield, 1998.
[90] D. Yildiz, et al., Thermal characterization of a R134A two-phase flashing jet, in: ICLASS 2003–9th International Conference on Liquid Atomization and Spray Systems, Sorrento, Italy, 2003.
[91] A. Kelsey, CFD Modelling of Two Phase Flashing Jets: Simulation of Flashing Propane jets, Health & Safety Laboratory Report, 2001, p. 61.
[92] A. Kelsey, CFD modelling of two phase flashing jets: simulation of evaporating sprays to inform modelling of flashing jet, Health and Safety Laboratory (1999) 56.
[93] M. Lopez_de_Bertolano, J.R.T. Lahey, O.C. Jones, Development of a k-e model for bubbly two-phase flow, Transaction of the ASME 116 (1994) 128–134.